Numerical Simulation of Flow in the Inlet Chamber of an Automotive Air Conditioning Condenser

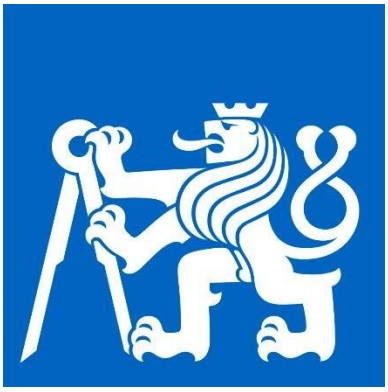

Czech Technical University in Prague

Faculty of Mechanical Engineering

Department of Fluid Mechanics and Thermodynamics

Egor Kalmykov

A bachelor's thesis submitted in partial fulfilment of the requirements for the award of the Degree of Theoretical Fundamentals of Mechanical Engineering

May 2024

BACHELOR'S THESIS ASSIGNMENT

I. Personal and study details

Student's name: **Kalmykov Egor** Personal ID number: **511034**

Faculty / Institute: **Faculty of Mechanical Engineering**

Department / Institute: **Department of Fluid Dynamics and Thermodynamics**

Study program: **Theoretical Fundamentals of Mechanical Engineering**

Branch of study: **No Special Fields of Study**

II. Bachelor's thesis details

Bachelor's thesis title in English:

Numerical simulation of flow in the inlet chamber of an automotive air conditioning condenser

Bachelor's thesis title in Czech:

Numerical simulation of flow in the inlet chamber of an automotive air conditioning condenser

Guidelines:

The bachelor thesis will be solved according to the following guidelines:
1) Perform a basic description of the automotive air conditioning system and its key components.
2) Describe the basic properties of numerical simulations in fluid flow (CFD) and the basics of the approach to the realization of numerical simulations (mesh quality, boundary conditions, calculation parameters, etc.)
3) Perform a numerical simulation of flow in two existing inlet channel geometries and evaluate their total pressure drop and the uniformity of flow through each condenser channel (simulate only the inlet part of the condenser).
4) Based on the simulation results, make your own innovative inlet geometry design.
5) Perform flow simulations in the new inlet geometry and evaluate the performance benefits of the new geometry.

Bibliography / sources:

According to the instructions of the bachelor thesis supervisor.

Name and workplace of bachelor's thesis supervisor:

Ing. Michal Schmirler, Ph.D. Department of Fluid Dynamics and Thermodynamics FME

Name and workplace of second bachelor's thesis supervisor or consultant:

Date of bachelor's thesis assignment: **15.04.2024** Deadline for bachelor thesis submission: **31.07.2024**

Assignment valid until: _____

Ing. Michal Schmirler, Ph.D. Supervisor's signature	Ing. Michal Schmirler, Ph.D. Head of department's signature	doc. Ing. Miroslav Španiel, CSc. Dean's signature

III. Assignment receipt

The student acknowledges that the bachelor's thesis is an individual work. The student must produce his thesis without the assistance of others, with the exception of provided consultations. Within the bachelor's thesis, the author must state the names of consultants and include a list of references.

Date of assignment receipt	Student's signature

Thesis Title: Numerical Simulation of Flow in the Inlet Chamber of an Automotive Air Conditioning Condenser

Author: Egor Kalmykov

Year: 2024

Study Program: Theoretical Fundamentals of Mechanical Engineering

Type of thesis: Bachelor's

Supervisor: Ing. Michal Schmirler, Ph.D.

Second supervisor/consultant: Ing. Jiři Stodulka, Ph.D.

Abstract: Two condenser inlet geometries have been given, with the task of evaluating performance with the use of Ansys Fluent CFD software. The two designs of the inlet to the manifold of the condenser were analysed and simulated using Ansys Fluent. Subsequently, on the basis of the findings, a new design was suggested and tested for improvements. The overall decrease in pressure drop in the suggested design was found to be 45,7% and 38,3% to the first and second given designs respectively. The absolute difference of maximum and minimum average mass flow rate per outlet was found to be 65,02% and 67,51% respectively.

Keywords: Condenser, Maldistribution, Fluent, Pressure Drop

Author's Affidavit

I hereby declare that the presented thesis, titled "Numerical Simulation of Flow in the Inlet Chamber of an Automotive Air Conditioning Condenser", made under supervision of Ing. Michal Schmirler, Ph.D., was written by me using literature listed in the chapter "Bibliography".

Date:.....

Signature:.....

Acknowledgements

I would like to thank Dr. Michal Schmirler and Dr. Jiři Stodulka for their expertise and all their help and support during the writing of this thesis. I would also like to thank Hanon Systems for the opportunity to conduct my research and write my thesis on the automotive condenser of their design. I would also like to thank my fiancée Lina, my family, and friends for supporting me over the course of the bachelor program and helping me to get to where I am today.

Introduction

The purpose of this thesis was to analyse the current performance of an automotive condenser and attempt to improve the geometry at the inlet to ensure a distribution of the flow in the inlet channel that is on par with the current design, or which offers an improvement in flow distribution, without compromising the pressure drop in the condenser itself. The topic of this thesis has been generously offered to the Department of Fluid Mechanics and Thermodynamics at FME CTU by Hanon Systems, who have provided the designs of current and potential inlet arrangements for their condenser. The area of interest for Hanon Systems was the jumper tube of the condenser, and whether it would be possible to eliminate it from the design without compromising performance. The purpose of the jumper tube is to direct the flow of refrigerant from the inlet flange to the main distribution channel. The condenser that serves as the basis for this thesis consists of a vertical header with fifty horizontal channels.

The condenser operates by pumping superheated refrigerant in gaseous state to the inlet of the condenser from the evaporator and directing it across the header towards numerous flat tubes, separated by corrugated louver fins. Air is then blown over these tubes by an external fan at different mass-flow rates, with the air taking the heat from the refrigerant and dispersing it to the ambient. The loss of heat by the refrigerant in the flat tubes causes the refrigerant to condense to a superheated liquid state, albeit at different rates and at different locations in the condenser. The refrigerant in the condenser tubes therefore presides predominantly in a mixed gaseous-liquid state. This applies restrictions on calculations and modelling during research, due to the complicated nature of mixed state fluids, and is outside of the scope of this thesis. The research for this thesis has been conducted assuming refrigerant existence in a fully gaseous state. The research procedure for this thesis consists of numerically evaluating flow distribution and pressure drop across two

condenser designs with given geometries, and to suggest an improved design, comparing it to the original two. The methodology of the thesis will include simulations using ANSYS Fluent on different geometries of the header and inlet in order to analyse and compare their performance. The thesis will attempt to outline potential changes and improvements that could be implemented to improve the overall performance and refrigerant distribution in the condenser.

Literature Review

From a thermodynamic stance, the HVAC system of any automotive vehicle is a vapor-compression cycle consisting of four distinct, interlinked parts, each performing a thermodynamic function to perpetuate and complete the cycle. These, in order, are the expansion valve, the evaporator, the compressor, and the condenser. Refrigerant flows through all these devices and presides in different states (or changes from one to another) in each one. Numerous types of refrigerants have been used in the past, with the most common one being R-134A. However, due to the environmental impact associated with the production and usage of the older refrigerants, most manufactures, mandated by EU regulations, have switched or are in the process of switching to newer, more environmentally friendly refrigerants such as the R-1234yf. This thesis utilises material properties of R-1234yf for refrigerant modelling.

As stated previously, refrigerant within the AC system flows from the expansion valve to the evaporator, then to the compressor, then the condenser, and then back to the expansion valve. The expansion valve decreases the pressure in the high-pressure liquid refrigerant coming from the condenser and allows it to expand. The refrigerant, now at a lower pressure, is sprayed into the evaporator where the refrigerant changes state from liquid to gas. The refrigerant does this by taking in the heat from the surroundings, cooling them, and evaporating in the process. The gaseous refrigerant then moves into the compressor, which enables the movement of

the refrigerant in the system. It does so by compressing the refrigerant gas, thereby increasing its pressure and temperature. The refrigerant gas then flows to the condenser, within which the superheated refrigerant flows through the condenser tubes and its heat is taken away, resulting in condensation.

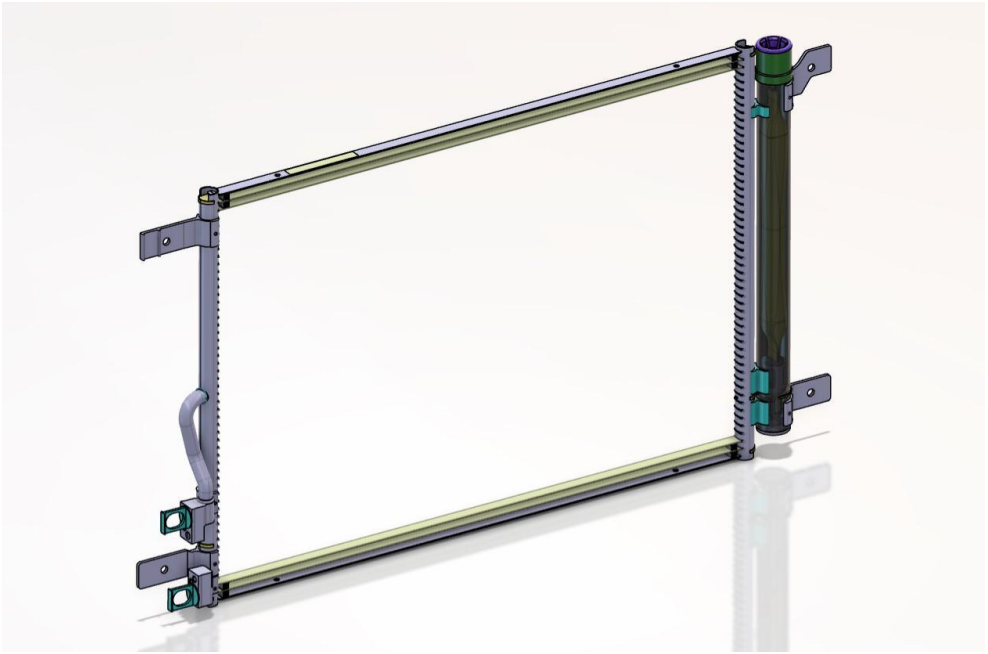

Figure 1 - Condenser analysed in this thesis, without the flat condenser tubes. The inlet manifold (which is to be simulated and analysed) is located on the left hand-side, along with the jumper tube and inlet flange.

The scope of this thesis will focus on the condenser itself. It is important to state that due to the similarity of the condenser and evaporator (both being heat exchangers and performing the same task in different order) numerous studies cited in the following pages draw upon their conclusions using experimental, analytical, and numerical data from evaporators and condensers.

The main distribution channel of the condenser, or header, can be modelled, and is in essence, a combined bifurcating and linear manifold. The flow separates initially and flows in two different directions (bifurcates), and then further separates into tubes along the manifold (separating linearly). The inlet tube which supplies the refrigerant to the header, depending on the design, will be located at different positions alongside it. Positioning of the inlet tube is vital to the performance of the condenser and can result in a varying distribution of the refrigerant to various

channels.[1] Generally, the supplied refrigerant is supplied best to the channels directly adjacent to, or those close to the inlet.[2]

Depending on the orientation of the header and the channels, gravity can also drastically alter the distribution of the refrigerant.[3] Along with the inertial and centrifugal forces, the resulting flow pattern attributed to these three forces alone results in a complex flow pattern.[4] In the case of a vertical header with horizontal tubes, the best location for the inlet to the header appears to be at the very top or bottom of the header, as shown by Shojaeefard et al. and Byun et al.[5] [6] This arrangement has been shown to result in the most even distribution of flow to all channels, albeit with a slight increase in pressure drop.

Due to the nature of liquid being supplied to each channel at different rates, maldistribution of flow in the condenser is almost guaranteed to occur, as according to analytical models, even flow distribution to the channels may only occur in the case that the header acts as an infinite reservoir. [7]

Maldistribution can lead to pressure drops of various severity, with potential reductions in performance and efficiency perhaps exceeding 30% and reducing

[1] Jin, D-H (2006). *Investigation on refrigerant distribution in evaporator manifolds*. [Doctoral Thesis, University of Maryland, College Park]. University of Maryland, College Park ProQuest Dissertations Publishing, 2006. 3222501, 16. https://www.proquest.com/openview/6678e938c207a5603c9bf1c46cfac0af/1?pq-origsite=gscholar&cbl=18750&diss=y

[2] Nagata, K., Katsuta, M., Kim, J. S., Sakuma, T. (Nov 1988). *Two Phase Flow Distribution in Serpentine Type Evaporator (First Report : Non-Heating Mode)*. KSME/JSME THERMAL and FLUID Engineering Conference, Seoul, South Korea, 212. https://www.dbpia.co.kr/Journal/articleDetail?nodeId=NODE00326727

[3] Huang, L., Lee, M. S., Saleh, K., Aute, V., Radermacher, R. (2014). A computational fluid dynamics and effectiveness-NTU based co-simulation approach for flow mal-distribution analysis in microchannel heat exchanger headers. *Applied Thermal Engineering*, *65*(1-2), 454.

[4] Kim, C.-H., Kim, N.-H. (2021). An experimental study of refrigerant distribution in an automotive condenser. *Applied Thermal Engineering, 184,* 116259, 4.

[5] Shojaeefard, M.S., Nourbakhsh, S.D., Zare, J. (2017). An investigation of the effects of geometry design on refrigerant flow mal-distribution in parallel flow condenser using a hybrid method of finite element approach and CFD simulation. *Applied Thermal Engineering*, *112*, 433.

[6] Byun, H., Kim, N. (2011). Refrigerant distribution in a parallel flow heat exchanger having vertical headers and heated horizontal tubes. *Experimental Thermal and Fluid Science*, *35*(6), 931.

[7] Bajura, R. A., Jones, E. H. (1976). Flow Distribution Manifolds. *Journal of Fluids Engineering*, *98*(4), 663.

capacity by up to 50%. [8] [9] [10] Maldistribution can likewise result in areas of high liquid loading, which can detrimentally affect heat transfer, and further reduce performance. Numerical and software analysis conducted by Brix et al. have both shown that maldistribution of flow negatively impacts the cooling capabilities of the whole AC system as a result. [11]

In summary, maldistribution results in reduced performance of the condenser. When maldistribution increases, the condensation rate of the condenser decreases, leading to lower amount of heat being taken away by the fan, therefore reducing cooling capability of the HVAC system. [12]

Inlet position is not the only deciding factor for maldistribution, however. Other factors that have been known to result in maldistribution include the geometry of the inlet, the geometry and length of the connection tube between the header and inlet (or lack thereof), point of supply of the refrigerant to the header, and header geometry and its positioning, among others. Any of these geometrical elements can be optimized to decrease maldistribution. Several studies show an improvement in results after geometrical optimization. Lee et al. have shown numerically that the supply of refrigerant at an angle of -21° at the y axis results in the most optimal distribution of refrigerant. [13] Specifically in the case of the shape of the tube cross-

[8] Choi, J. M., Payne, V., Domanski, P. A. (2003, August 17-22). *Effects of Non-Uniform Refrigerant and Air Flow Distributions on Finned Tube Evaporator Performance*. Refrigeration International Congress, 21st IIR. (IRC2003). 10th Technical Session Energy-Efficient Heating and Cooling Systems for Buildings, Washington, DC, USA, 8. [online], https://tsapps.nist.gov/publication/get_pdf.cfm?pub_id=101203 (Accessed May 21, 2024).
[9] Zou, Y., Tuo, H., Hrnjak, P S. (2014). Modeling refrigerant maldistribution in microchannel heat exchangers with vertical headers based on experimentally developed distribution results. *Applied Thermal Engineering*, *64*(1–2), 180.
[10] Lalot, S., Florent, P., Lang, S. K., Bergles, A. E. (1999). Flow maldistribution in heat exchangers. *Applied Thermal Engineering*, *19*(8), 863.
[11] Brix, W., Kærn, M. R., Elmegaard, B. (2009). Modelling refrigerant distribution in microchannel evaporators. *International Journal of Refrigeration*, *32*(7), 1743.
[12] Rao Bobbili, P., Sunden, B., Das, S. K. (2006). Thermal analysis of plate condensers in presence of flow maldistribution. *International Journal of Heat and Mass Transfer*, *49*(25–26), 4976.

[13] Lee, K-S., Oh, S-J. (2004). Optimal shape of the multi-passage branching system in a single-phase parallel-flow heat exchanger. *International Journal of Refrigeration*, *27*(1), 85.

section, the geometry itself seems to have the most significant effect on maldistribution, with flat tubes having better accuracy for numerical solutions.[14]

Habib et al. and Rao et al. have further expanded on these findings, indicating the geometry, diameter, and number of channels as the factors associated with increased maldistribution. [15] [16] Alterations to the mass flow rate at the inlet, as well as the inlet flow velocity, seem to have almost no effect on maldistribution, but lower mass flow rate may result in more uniform flow.[17] [18] Zou et al. and Zou et al., however, have made findings contrary to those mentioned above. They discovered that flow distribution improves with increased mass-flow rate.[19] [20] The academic consensus on this is therefore unclear. While not directly influencing maldistribution, refrigerant vapour quality likewise affects performance by decreasing pressure drop.[21] Another geometrical factor that has been shown to increase pressure drop and result in increased maldistribution is the tube protrusion depth into the header. By increasing protrusion depth from ¼ of the header diameter to ¾, the pressure drop increases by 14%, and capacity of the condenser decreases by 3,9 %. The decreased area for the passage of flow, therefore, is another cause of flow maldistribution.[22]

[14] Chung, K., Lee, K-S., Kim, W- S. (2002). Optimization of the design factors for thermal performance of a parallel-flow heat exchanger. *International Journal of Heat and Mass Transfer*, *45*(24), 4780.
[15] Habib, M., Ben-Mansour, R., Said, S., Al-Qahtani, M., Al-Bagawi, J., Al-Mansour, K. (2009). Evaluation of flow maldistribution in air-cooled heat exchangers. *Computers & Fluids*, *38*(3), 689.
[16] Rao, B. P., Das, S K. (2004). An Experimental Study on the Influence of Flow Maldistribution on the Pressure Drop Across a Plate Heat Exchanger. *Journal of Fluids Engineering*, *126*(4), 691.
[17] Vist, S., Pettersen, J. (2004). Two-phase flow distribution in compact heat exchanger manifolds. *Experimental Thermal and Fluid Science*, *28*(2–3), 212.
[18] Tompkins, D. M., Yoo, T., Hrnjak, P., Newell, T., Cho, K. (2002). Flow Distribution and Pressure Drop In Microchannel Manifolds. *International Refrigeration and Air Conditioning Conference*, *Paper 554*, Purdue University, 5.
[19] Zou, Y., Hrnjak, P S. (2013). Experiment and visualization on R134a upward flow in the vertical header of microchannel heat exchanger and its effect on distribution. *International Journal of Heat and Mass Transfer*, *62*, 133.
[20] Zou, Y., Hrnjak, P. S. (2013). Refrigerant distribution in the vertical header of the microchannel heat exchanger – Measurement and visualization of R410A flow. *International Journal of Refrigeration*, *36*(8), 2207.
[21] Shojaeefard, M., Molaeimanesh, G., Yarmohammadi, A., Changizian, S. (2017). Multi-objective optimization of an automotive louvered fin-flat tube condenser for enhancing HVAC system cooling performance. *Applied Thermal Engineering*, *125*, 555.
[22] Shojaeefard, M. H., Nourbakhsh, S. D., Zare, J. (2017). An investigation of the effects of geometry design on refrigerant flow mal-distribution in parallel flow condenser using a hybrid method of finite element approach and CFD simulation. *Applied Thermal Engineering*, *112*, 445.

This has been further shown by Choi et al., having demonstrated that the area ratio, or the ratio of cross-sectional area of the header across flow to the cross-sectional area of the header along flow, is optimal when it is equal to 4, further underlining the importance of having sufficient passage area of the flow.[23] It must be stated that, due to space limitations with an automotive vehicle, this is not always achievable. However, using the findings by Datta et al., which show that the automotive condenser tube length can in some cases be significantly reduced provided the necessary condensation and heat transfer rate can be preserved, a more proliferated use of adequately suitable area ratios is feasible.[24]

As stated previously, maldistribution is caused by, at least in part, the pressure drop in the header. Ting et al. and Habib et al., among others, state that is in fact the single most important factor resulting in maldistribution.[25] [26] [27] [28]

Alternatively, specific alterations to the design of the header and the inlet tube can result in an increase of heat transfer by 55%.[29] This subsequently results in improvement of the condensation rate, and an increase in performance of the condenser as a whole. Good performance of the condenser translates into a better functioning AC system, reduced emissions, and even better fuel economy. There is evidence to suggest that maldistribution can be minimised to some degree by the level of disturbance of a chaotic flow at the inlet.[30]

[23] Choi, S. H., Shin, S., Cho, Y. I. (1993). The effect of area ratio on the flow distribution in liquid cooling module manifolds for electronic packaging. *International Communications in Heat and Mass Transfer*, *20*(2), 233.
[24] Datta, S., Das, P., Mukhopadhyay, S. (2016). Performance of a condenser of an automotive air conditioner with maldistribution of inlet air—Simulation studies and its experimental validation. *International Journal of Heat and Mass Transfer*, *98*, 378.
[25] Wang, T., Gu, B., Wu, B., Ma, H., Qian, C. (2015). Modeling for multi-pass parallel flow condenser with the effect of refrigerant mal-distribution. *International Journal of Refrigeration*, *60*, 234.
[26] Habib, M., Ben-Mansour, R., Said, S., Al-Qahtani, M., Al-Bagawi, J., Al-Mansour, K. (2009). Evaluation of flow maldistribution in air-cooled heat exchangers. *Computers & Fluids*, *38*(3), 677.
[27] Tuo, H., Hrnjak, P. (2013). Effect of the header pressure drop induced flow maldistribution on the microchannel evaporator performance. *International Journal of Refrigeration*, *36*(8), 2186.
[28] Thonon, B., Mercier, P., Feidt, M. (1992). *Flow Distribution in Plate Heat Exchangers and Consequences on Thermal and Hydraulic Performances.* In: Roetzel, W., Heggs, P.J., Butterworth, D. (eds) Design and Operation of Heat Exchangers. EUROTHERM Seminars, vol 18. Springer, Berlin, Heidelberg, 245.
[29] Lee, K. S., Oh, S. J. (2004). Optimal shape of the multi-passage branching system in a single-phase parallel-flow heat exchanger. *International Journal of Refrigeration*, *27*(1), 87.
[30] Vist, S., Pettersen, J. (2004). Two-phase flow distribution in compact heat exchanger manifolds. *Experimental Thermal and Fluid Science*, *28*(2–3), 215.

One way that manufacturers attempt to circumvent maldistributions of the refrigerant is to incorporate several passes of the refrigerant along the tubes. The pass number is usually an even number. Multiple passes allow the refrigerant to condense more evenly and homogeneously. This is due to the more uniform flow that forms as a result of multi-pass implementation. Kim et al. concluded that the optimal number of passes depends on the inlet diameter and is proportional to it.[31] Automotive HVAC manufacturers, and the manufacturers of HVAC systems at large tend to implement two passes in their condensers. Results obtained by Zhou et al. show an increase in condenser pressure drop in the cases that four or more passes are implemented.[32]

Potential further reduction of maldistribution might be achieved by separating the condenser into more cooling zones, instead of the traditional four.[33] Shojaefaard et al. have shown that alterations to louvered fin pitch may further reduce pressure drop in the condenser.[34]

Header pressure drop can be reduced by increasing the superheated temperature of the supplied refrigerant.[35]

It can be concluded form these findings that the primary parameters that need to be monitored and reduced to a minimum are the pressure drop within the header and the maldistribution of flow. To that end, the following section describes the means of measurement used in this thesis.

[31] Kim, M. S., Lee, K. S., Song, S. (2008). Effects of pass arrangement and optimization of design parameters on the thermal performance of a multi-pass heat exchanger. *International Journal of Heat and Fluid Flow*, *29*(1), 362.
[32] Zhao, Y., Liang, Y., Sun, Y., Chen, J. (2012). Development of a mini-channel evaporator model using R1234yf as working fluid. *International Journal of Refrigeration*, *35*(8), 2176.
[33] Li, W., Tu, J., Liu, Y., Wang, D., Shi, J., Chen, J. (2021). Design and experimental validation of a new condenser of an automotive air conditioning unit to address non-uniform air velocity distributions. *International Journal of Refrigeration*, *131*, 834.
[34] Shojaeefard, M., Molaeimanesh, G., Yarmohammadi, A., Changizian, S. (2017). Multi-objective optimization of an automotive louvered fin-flat tube condenser for enhancing HVAC system cooling performance. *Applied Thermal Engineering*, *125*, 554.
[35] Yan, Y. Y., Lin, T. F. (1999). Condensation heat transfer and pressure drop of refrigerant R-134a in a small pipe. *International Journal of Heat and Mass Transfer*, *42*(4), 707.

Data Collection

Data collection for this thesis has been conducted via numerical solution simulation using ANSYS Fluent. Fluent is a versatile tool, allowing for detailed hydro and thermodynamic simulations for any input geometry given by the user. Fluent achieves this by discretization of the geometry into separate finite elements (cells) through which the flow will be calculated, and by utilizing a hierarchy of flow equations that are then numerically solved within the resulting cell-constructed geometry (mesh).

The first matter to be considered is the geometry of the manifold and the tubes. For the purposes of this thesis, the volume region of the design geometry has been extracted, to reduce computational cost. The outlet channels of the condenser have been shortened, for the same reason. Only the part of the inlet manifold within which the refrigerant is in its gaseous state was considered and simulated. The first, original design to be evaluated consists of a jumper tube connecting the inlet flange to the manifold, with the manifold inlet being located 2/5ths of the way down from the top

of the manifold when viewed normally. This design, in principle, should allow the flow to bifurcate relatively evenly to either side of the manifold.

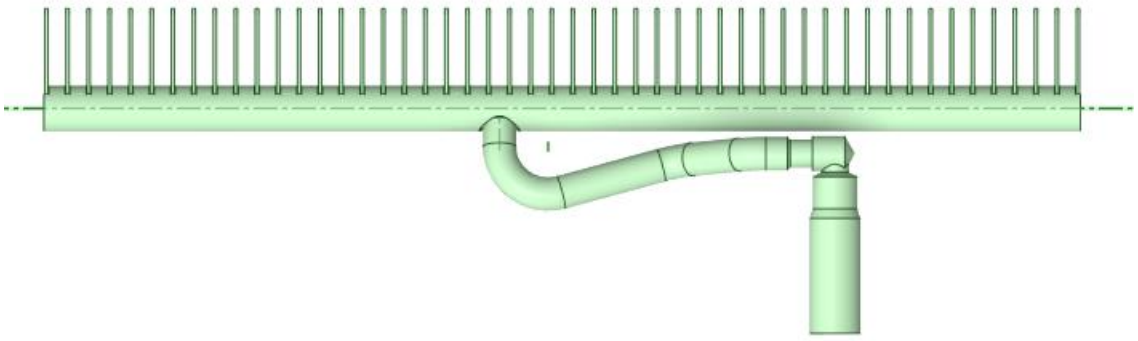

Figure 2 - Extracted fluid region of the manifold, jumper tube, inlet, and parts of the flat tubes of the original condenser design.

The second design consists of a much shorter, straight tube with a stadium-shaped cross section projected at an angle from the inlet flange towards the manifold and connecting with it just over 3/5ths of the way down from the top of the manifold.

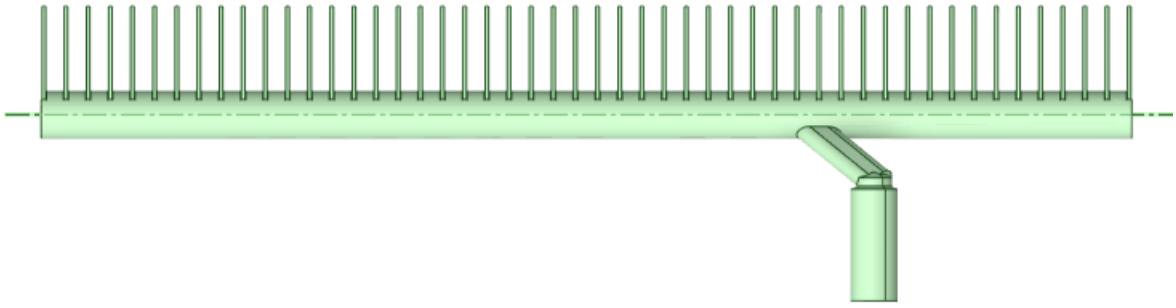

Figure 3 - Extracted fluid region of the manifold, jumper tube, inlet, and part of the condenser tubes of the second design.

Numerous suggested designs have been developed, considering the findings of previous research conducted on the topic. Designs that incorporated jumper tubes connecting to the very top of the manifold (as conducted by Shojaeefard et al. and Byun et al.), as well as designs with the jumper tube connected at -21° from the y-axis of the manifold (as conducted by Lee et al.), among others, have been developed and tested. These designs haven not managed to attain the expected results.

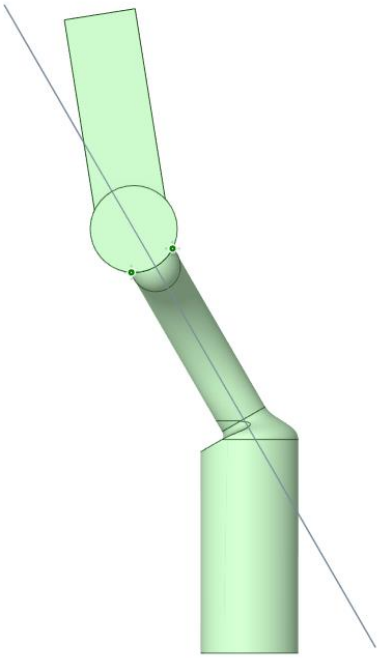

Figure 4 - Side view of a tested, unused design created according to findings of Lee et al., with the jumper tube connected to the manifold at an angle of -21 degrees from the y-axis.

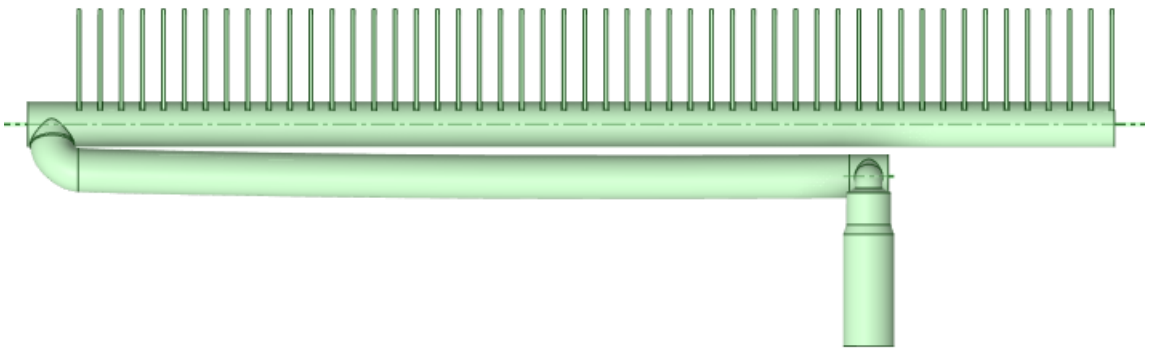

Figure 5 - Unused design created according to the findings of Shojaeefard et al. and Byun et al.

The geometry that has been determined to have the most potential was a design utilising a jumper tube extruded over a curve with radius of $\frac{\pi}{2}$ in the xy plane, which passes through the axis of symmetry of the inlet. The jumper tube is then further extruded forward to connect to the manifold perpendicularly to the outlet tubes, -1.2mm from the axis of the manifold.

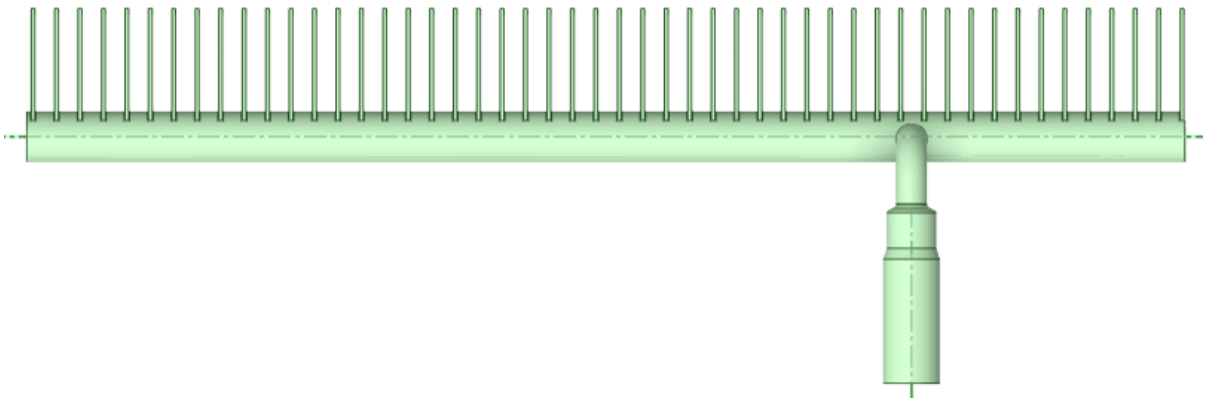

Figure 6 - Frontal view of the suggested design.

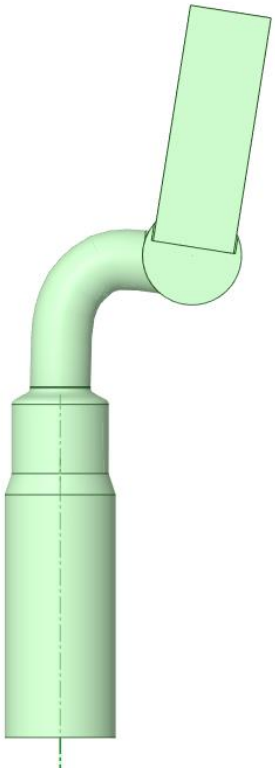

Figure 7 - Side-view of the suggested design.

The finite elements, or cells, are generated by applying restricting conditions on the algorithm in order to generate the desired resulting arrangement of cells, or a mesh. These conditions include the selection of the cell shape, minimal and maximal cell size, growth rate (or rate at which the cells get larger with each subsequently generated cell), size and proximity functions and more.

Cell size and shape are the most important factors. The mesh size must be fine enough to accurately replicate the geometrical details and intricacies of the CAD model to ensure the most accurate result, but not too fine, where further decreases in mesh size do not result in improved accuracy and only lead to longer processing time and higher computational requirements and cost. Mesh shape determines the accuracy of the simulation as well. 2D mesh is restricted to 2D polygons, most usually triangles, square, and hexagons. 3D mesh elements can be tetrahedral, hexcore, polyhedral, or poly-hexcore.

The mesh is generated in Fluent procedurally, by completion of several defined steps within the defined workflow in Fluent.

The first step in generating a mesh is importing the geometry into Fluent. After the geometry has been imported, the next step is the generation of the surface mesh. The surface mesh is a mesh that is created on the surface of the CAD model to capture the geometrical elements and intricacies of the geometry. The surface mesh is used to define the computational fluid domain within which the calculations will be processed. The mesh should contain no gaps or openings, as Fluent will not be able to generate a volume mesh in their presence. The inlets and outlets should therefore be identified within the workflow to be “capped”; to have a mesh generated over the openings. The mesh should be further refined to ensure all faces have been properly and accurately represented by the generated mesh, and that no mesh cells have been badly generated or skewed.

The minimum and maximum cell size for mesh generation was set to be 0.05 and 1.2 mm respectively. This mesh size allowed for the creation of a mesh of good quality, without compromising technical performance.

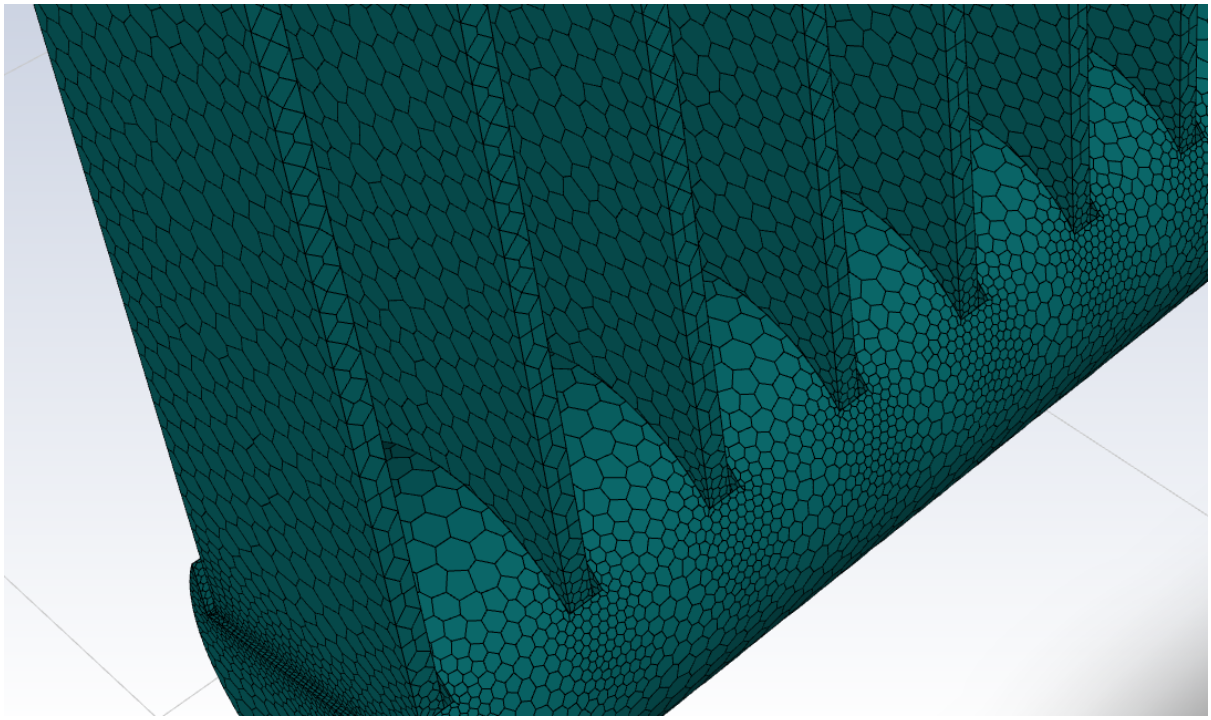

Figure 8 - Example of the generated surface mesh.

The mesh size was tested and determined to be sufficiently fine for simulation purposes. Cell skewness was shown to not exceed 0.59 (the standard Fluent limit for cell quality being <0.6).

A subsequent mesh generation step of high importance is the setting of boundary layers. Boundary layers are thin layers of cells that are formed along the edges of the fluid region, at and near the point of contact of the fluid with the solid geometry. As flow at the boundaries of the fluid region differs significantly from the flow elsewhere within it, the boundary layers are necessary to simulate more precisely the flow behaviour at those surfaces. Four layers were chosen as an adequate number of layers for good resolution of flow at the boundary.

For the volume mesh generation process, the settings were set for the formation of the mesh with polyhedral cells with a maximum length of 1.2 mm, and a growth rate of 1.2. The growth rate is the rate of cell growth on the inflation layers of the cells. In essence, the cells grow in size with each successive layer. This is done in order to reduce computational time and cell number, as some regions do not require the mesh to be as precise as other parts. To restrict stair-stepping, a phenomenon by which the Fluent program attempts to generate triangular prism cells on the inflation

layers in some locations, non-default stair-step handling has been enabled. This was done to prevent mesh deterioration.

Once the mesh has been generated it can be evaluated for quality. A cross-sectional cut through the zy plane showed that the quality of the generated cells was satisfactory. All geometrical parameters of the fluid region mesh were preserved, and the generation process produced the desired boundary layers.

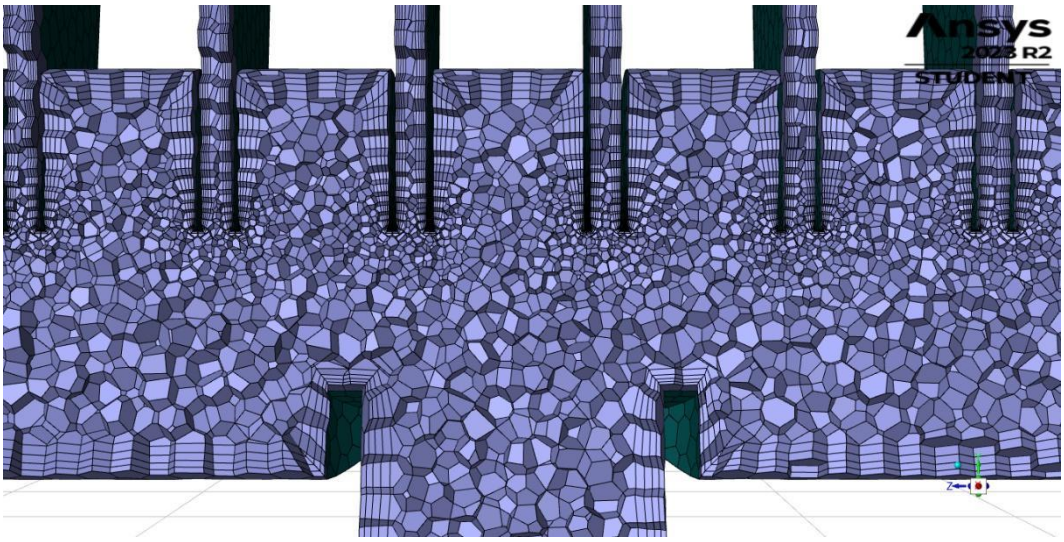

Figure 9 - Cross-sectional view of the generated mesh, displaying the generated cells and boundary layers.

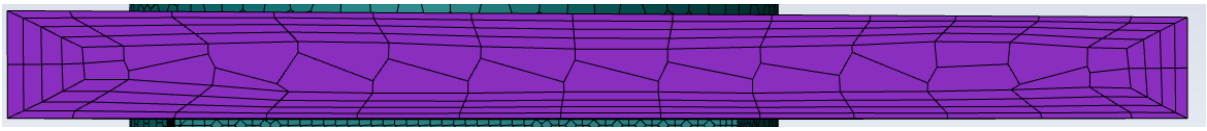

Figure 10 - Top-down view of the generated boundary layers (concentric profiles along the edges) and fluid region cells.

All mesh models have been generated with cell count approximately between 850000 – 1040000.

Setting the correct parameters for simulation was the next step. Fluent uses the common flow-governing equations (such as the mass and energy conservation laws, compressible and incompressible Navier-Stokes equations, and turbulence equations) and solves them using the finite volume method. This method consists of taking the conservative variants (where fluxes, both incoming and outgoing, on the

boundary between two adjacent volumes are identical) of the equations and solving them over a discrete finite volume. This method allows to most closely simulate the flow of fluid in the real geometry within a discrete model.

Turbulence models are another core feature that must be paid due attention. The turbulence model, in simulations where laminar flow cannot be assumed, determines the overall outcome of the simulation, and its accuracy. Since the Reynold's numbers attained during calculation have been shown to range from laminar to turbulent, choosing a suitable turbulence model becomes ever more important. Turbulence is modelled using mathematical equations to determine the flow within the flow field. The two most common methods used are the Reynolds-Averaged-Navier-Stokes (RANS) and Large Eddy Simulation (LES) models. The RANS model utilises Reynolds decomposition to simulate turbulence, by which the instantaneous, time-averaged quantities of the flow are broken into the expectant and fluctuation values, with the former being used in calculating the Navier-Stokes equations. The LES model utilises a wide range of length and time scales when numerically solving the Navier-Stokes equations. This wide range of values used in calculations, even when paired with the low pass filtering of the smallest intervals (as is common practice) leads to very high computational costs. Within Fluent, the RANS model is used.

The most common RANS approaches used in Fluent are the k-models, k standing for the turbulent kinetic energy of flow. The $k-\omega$ model uses the k and ω (specific dissipation rate), and two equations to calculate eddy viscosity. The $k-\varepsilon$ model once again uses the k, but instead of the specific dissipation rate ω, it uses dissipation rate ε. The $k-\varepsilon$ model has been shown to be satisfactory when it comes to modelling engineering applications.[36] The simulation can be further improved by use of the realisable $k-\varepsilon$ model, which accounts for non-isotropic effects, and has better handling of vortices and streamline curvature of the flow field.[37] The realizable $k-\varepsilon$

[36] Shirzadi, M., Mirzaei, P. A., Naghashzadegan, M. (2017). Improvement of k-epsilon turbulence model for CFD simulation of atmospheric boundary layer around a high-rise building using stochastic optimization and Monte Carlo Sampling technique. *Journal of Wind Engineering and Industrial Aerodynamics*, *171*, 367.

[37] Liu, M., Jiang, C., Khoo, B. C., Zhu, H., Gao, G. (2024). A cell-based smoothed finite element model for the analysis of turbulent flow using realizable k-ε model and mixed meshes. *Journal of Computational Physics*, *501*, 2.

model is the turbulence model that has therefore been chosen for the following simulations.

As stated previously, the refrigerant used within the AC system is R-1234yf, with the chemical composition 2,3,3,3-Tetrafluoropropene. The manufacturer of R1234yf – Opteon – does not list the thermodynamic properties above 80 °C.[38] From the increases in density, it is evident from the tables that the density at 105 °C would be $\rho \approx 500\ kg/m^3$. The value of 470.9 kg/m^3 is used in the calculations, corresponding to the density of the gas at 94.8 °C, as listed by Honeywell Inc.[39] Dynamic viscosity, as listed by Honeywell Refrigerants Inc., is $1.15 \cdot 10^{-5}\ kg/m \cdot s$.[40] Data used by Huber et al. is in agreement with this value.[41]

To conduct the simulations, the boundary conditions at the inlet and outlet must be set and defined. Generally, the parameters to be used at the inlet and outlet may vary, so long as the flow within the system can be calculated.

The boundary condition at the inlet was chosen to be set as Mass Flow Inlet. Mass flow is the main test parameter by which the condenser has been evaluated in the past, and it is therefore appropriate to utilize it for the simulations as well. The condenser has been tested previously on range of mass-flow rates, but for the sake of comparative analysis between the simulations it has been decided to use the average value that has been used in testing before – 180 kg/h. Converting to SI units, the mass flow rate becomes $\dot{m} = 0.05$ kg/s. The other parameters at the inlet are left as default.

The boundary condition at the outlet was chosen to be set as an Outlet Vent. The Outlet Vent boundary condition functions like a Pressure Outlet, but with a pressure

[38] The Chemours Company FC, LLC. (2018). *Thermodynamic Properties of Opteon™ YF*. https://www.opteon.com/en/-/media/files/opteon/opteon-yf-thermodynamic-properties-si.pdf?rev=8fa3ce05a4fa4573b9b6750afebecd0e

[39] Honeywell Inc. *HFO-1234yf - Thermodynamic Properties – IP units*. https://www.rsd.net/fx/pdf/suite/honeywell_genetron/Genetron_HFO-1234YF_PT_Chart.pdf

[40] Honeywell Refrigerants Inc. (2015, May). *Solstice® yf Properties and Materials Compatibilit*y. https://www.honeywell-refrigerants.com/europe/wp-content/uploads/2015/06/Solstice-yf-Properties-and-Materials-Capatibility-060115.pdf

[41] Huber, M. L., Assael, M. J. (2016, November). Correlations for the viscosity of 2,3,3,3-tetrafluoroprop-1-ene (R1234yf) and trans-1,3,3,3-tetrafluoropropene (R1234ze(E)). *International Journal of Refrigeration*, *71*, 43.

loss coefficient applied to it. This was done to more closely simulate the flow to what it would be expected to be in the condenser. The length of the tubes within the condenser is approximately 500mm, whereas the length of the tubes within the model is 33 mm. It was therefore necessary to implement a pressure loss coefficient to account for this difference. The Outlet Vent condition can only be used in Fluent under the condition that the temperature is constant. All flow within the simulation is therefore taken to be isothermal.

The pressure loss coefficient can be calculated from the Darcy-Weisbach formula for calculating pressure drop:

$$\Delta p = (f_D \frac{L}{D_H}) \frac{\rho v^2}{2}$$

Where: Δp – pressure drop, f_D – friction factor, L – pipe length, D_H – hydraulic diameter, ρ-density, v – mean flow velocity.

In this equation, the product of the terms $f_D \frac{L}{D_H}$ is equal to the pressure loss coefficient k_L.

The Outlet Vent boundary condition allows the user to specify the loss coefficient by setting it to be constant, polynomial, piecewise-linear or piecewise-polynomial. In all setting cases apart from constant, the loss coefficient becomes a function of velocity passing through the outlet. Within a physical condenser, the loss coefficient can never be the same for all the tubes, regardless of the conditions. The constant loss coefficient could therefore not be applied to the simulations. The polynomial setting has therefore been chosen as the most appropriate.

The velocity has been determined from initial testing to be within the range of 0.01 – 3.6 m/s. To determine the polynomial equation to be used in Fluent, several velocity values within the range were input into the Reynolds number formula for Newtonian fluids:

$$Re = \frac{\rho v D}{\mu}$$

Where: ρ – density, v – velocity of flow, D – characteristic dimension, μ – dynamic viscosity.

The calculated values were then input into the Blasius equation for turbulent flow within a smooth pipe to calculate the friction factor f_D:

$$f_D = \frac{0{,}316}{Re^{\frac{1}{4}}}$$

The value for 0,01 m/s, however, was instead input into the equation:

$$f_D = \frac{64}{Re}$$

This was done as the flow would be laminar at such low Reynold's number values. The values of the friction factor for the laminar flow would hence be higher than the friction factor for turbulent flow.

The constant values that were used in the aforementioned equations are:

L	0,534 m
ρ	470,9 kg/m^3
D	0,001 m
D_H	0,001 m
μ	0,0000115 Pa/s

Figure 11 - Table of constants utilized in the calculations.

The resulting friction factors were then used to calculate k_L. The results of the calculations are listed in the table in Figure 12.

v [m/s]	Re [-]	f_D [-]	k_L [-]
0,01	434,78	0,1472	78,6048
0,6	26086,96	0,024865	7,2161
1,2	52173,91	0,020909	6,068022
1,8	78260,87	0,018893	5,483077
2,4	104347,83	0,017582	5,102578
3,0	139434,78	0,016628	4,82572
3,6	156521,74	0,015887	4,6107

Figure 12 - Results of the calculation of the pressure loss coefficient k_L for a range of velocities.

The values of the loss coefficient k_L can then be plotted against the values of velocity, and the equation of the resulting curve is the polynomial equation that may be used in Fluent for pressure loss coefficients.

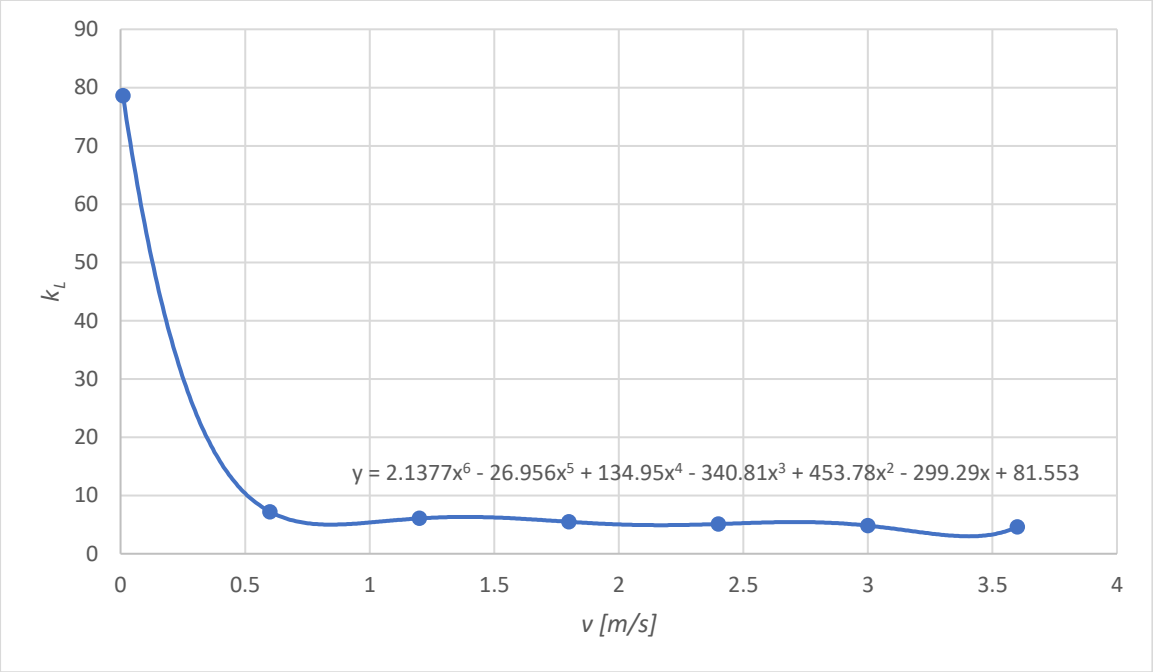

Figure 13 - Polynomial equation for the pressure loss coefficient k_L.

The final polynomial equation to be used is:

$$y = 2{,}1377x^6 - 26.956x^5 + 134{,}95x^4 - 340.81x^3 + 453{,}78x^2 - 299{,}29x + 81.553$$

The other settings at the outlet have been left as default.

Within the operating conditions tab, the operating pressure is set to 1.9 MPa. Real-world tests of the condenser have utilized this value previously as the condensation pressure. To account for gravitational effects with respect to the orientation of the condenser within an automotive vehicle, the Gravity parameter was turned on, and the magnitude of gravitational acceleration was set to -9.81 m/s² along the z-axis.

To monitor the necessary parameters by which the simulations are to be evaluated and compared, the definitions and plots were set for the mass-flow rate and average area-weighted pressure at each outlet. An additional average area-weighted plot was likewise created at the inlet. A final plot consisting of the average area-weighted pressure over all the outlets was defined to be used to assess pressure drop.

Each simulation was then initialized for 10 iterations. Initialization in CFD modelling refers to cells being assigned a value that the solver "guesses" for each iteration. This is done to assess how fast convergence of solutions can be reached. Finally, each simulation was set for 1000 iterations and calculated. 1000 iterations were arbitrarily chosen as the value by which all simulations have reached convergence.

Analysis

The simulations were completed in the following order: the original design was tested first, followed by the design suggested by Hanon Systems, followed finally by the suggested design produced by the student. The simulations and their results are analysed in order.

First, it is important to assess whether the solution has converged. Convergence within CFD modelling mainly refers to whether the residuals have reached a certain threshold. This threshold differs from the standard convergence criteria employed within the mathematical and computer engineering works, where the convergence criterion can be as low as the machine tolerance of the computational device. Additionally, it is evaluated whether the residuals are decreasing further or not; if the residuals are small enough, and the residuals are no longer decreasing, then it is said that the solution has converged. The residuals are produced as a result of solving of the transfer equations within Fluent over the course of the iterative solution. The smaller the convergence – the more accurate the result will be. Generally, the solution is said to have converged if the residuals have decreased to the 10^{-3} orders of magnitude. This is not always possible however, as the reduction in residual values is a direct consequence of the initial "guess" of the reduction in said residuals prior to the calculation. If the guess was not close enough, the reduction of the residuals will be different. Stabilization of the values in other monitors can also signify convergence, even if the threshold for residual reduction has not been reached.

The following residuals of the solution of the first design were produced:

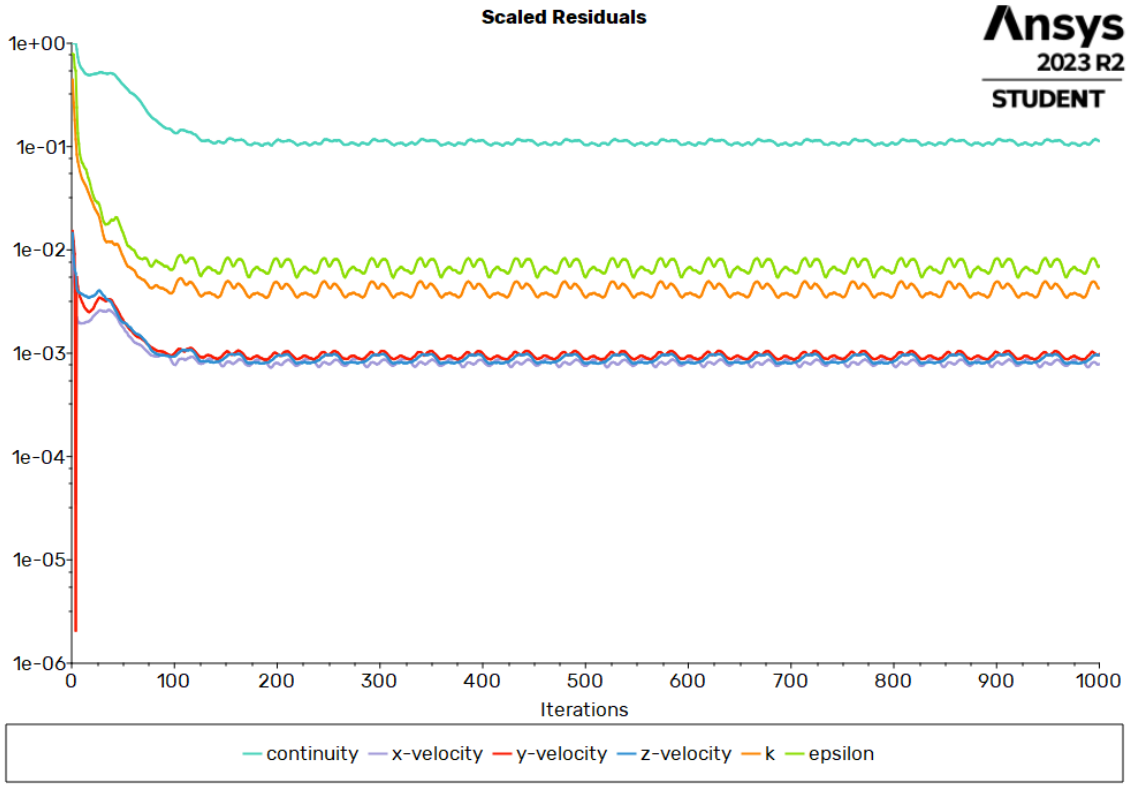

Figure 14 - Residuals of the simulation of the original design.

It is possible to see that the continuity residuals have not decreased to the desired threshold, but have stabilized, oscillating around set values.

The graph of the total inlet pressure monitored over 1000 iterations has likewise stabilized:

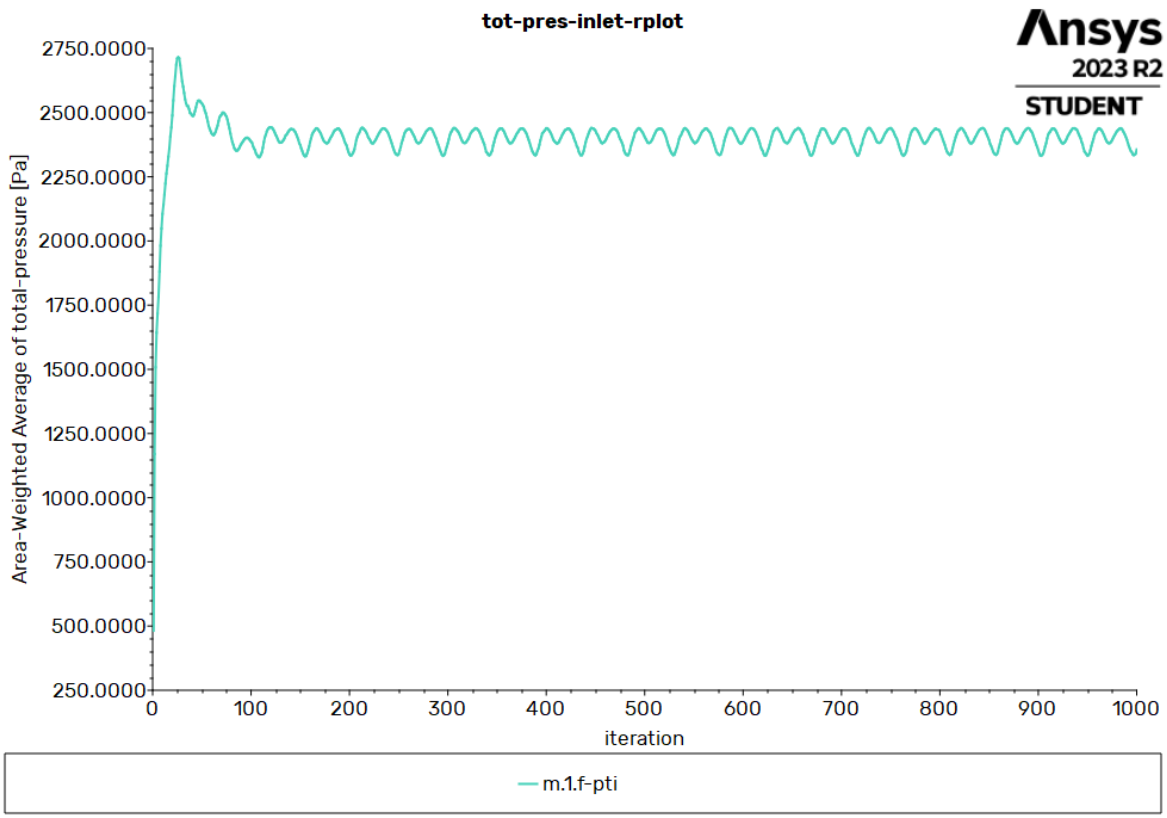

Figure 15 - Monitor of the total pressure at the inlet of the original design over 1000 iterations.

With the stabilization being a good sign of convergence of the solution. Furthermore, the resulting total pressure at the inlet can be measured to be 2375,45 ± 51.35 Pa.

The total pressure distribution monitor for separate outlets has produced the following graphical result:

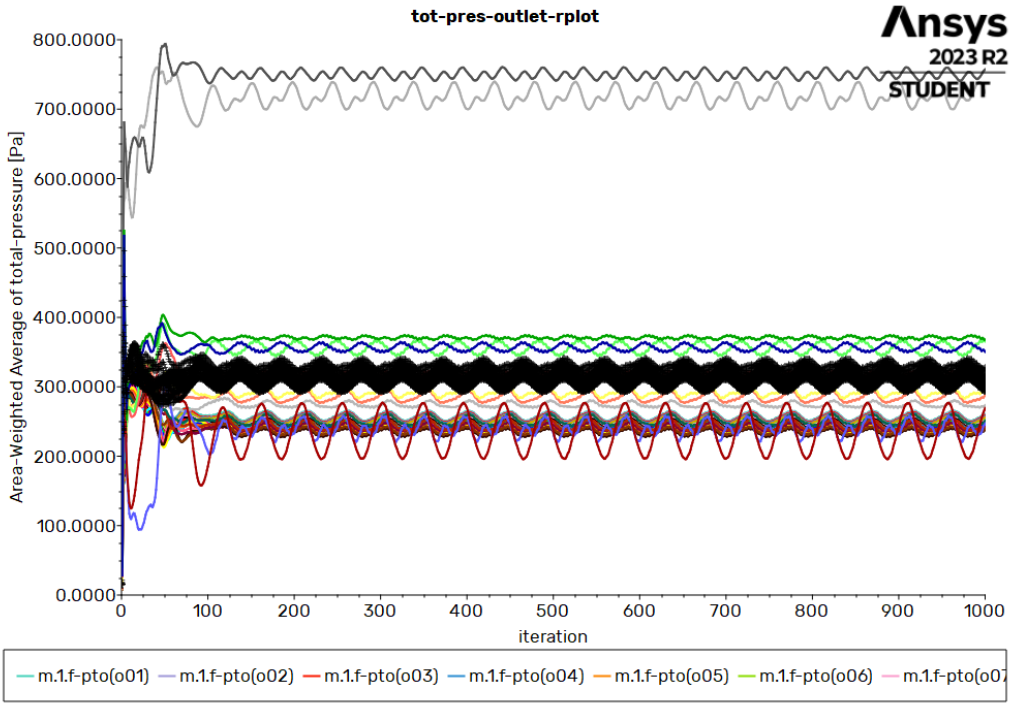

Figure 16 - Monitor of the total pressure in every outlet channel of the original design, over 1000 iterations.

It is possible to see that two outlet channels had higher total pressure than the rest – those outlets being channels 28 and 29, located directly above the inlet to the manifold.

The average total pressure at the outlets has produced the following graphical result:

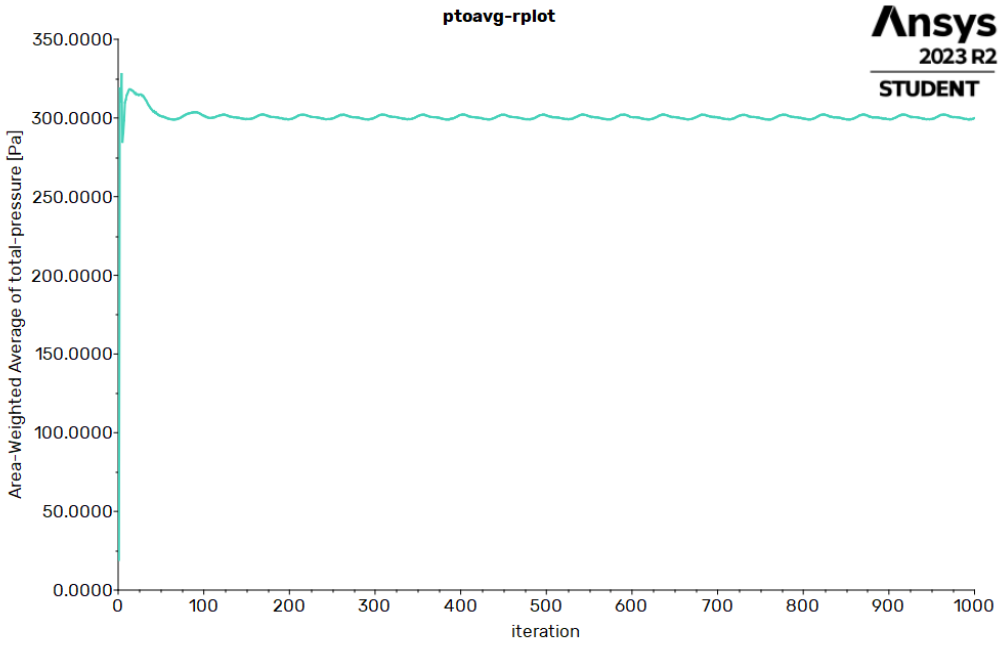

Figure 17- Monitor of the total average pressure over all 50 outlets of the original design, over 1000 iterations.

The mean outlet pressure has been measured to have a value of 300,55 ± 1,52 Pa after 1000 iterations.

Therefore, the average pressure drop Δp within this manifold design can be calculated to be: $\Delta p_{avg} = p_{in} - p_{outavg}$ = 2074,90 ± 52,86 Pa.

Creating the total pressure contours within the model allows for the pressure distribution to be evaluated graphically:

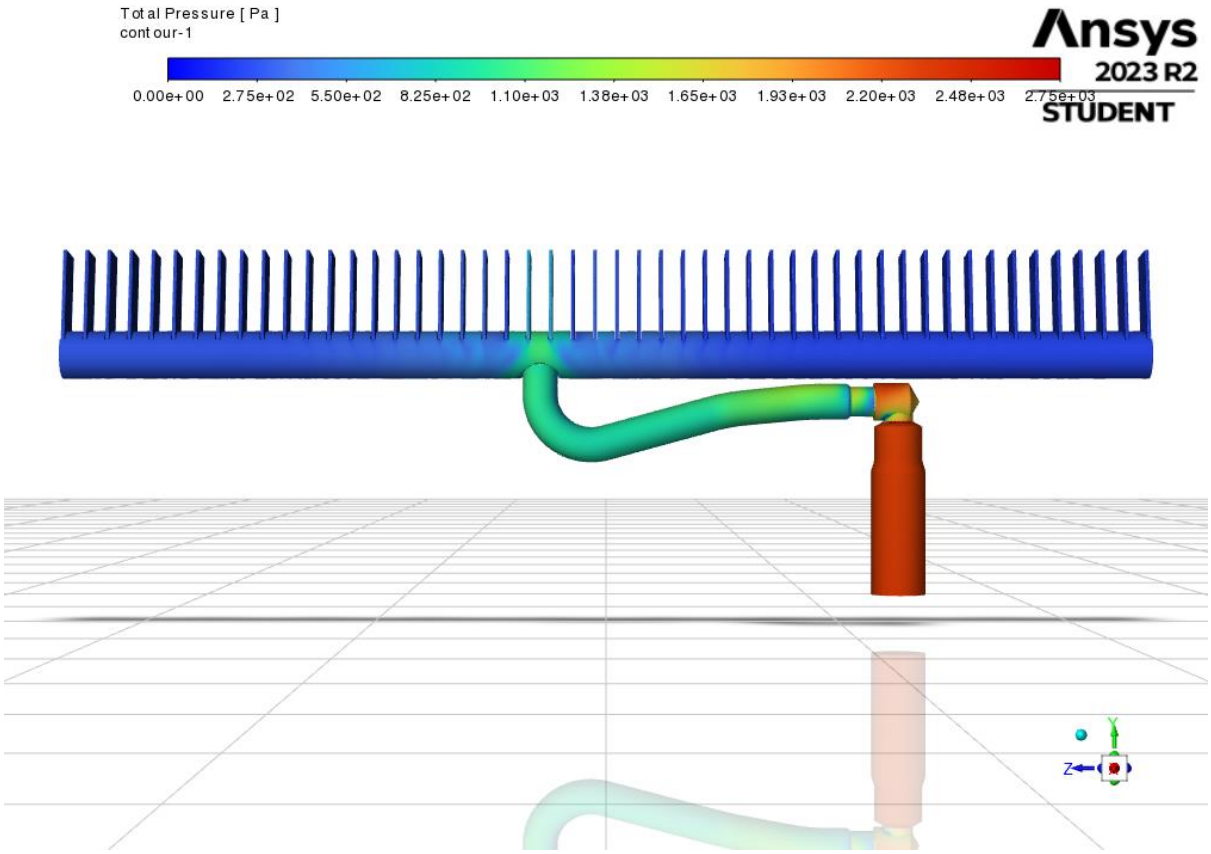

Figure 18 - Frontal view of the original design, displaying the total pressure distribution.

As expected, the highest pressure was present in the inlet flange of the condenser. The channel contraction, and the wall at the very end of the inlet flange caused the flow to exert higher pressure in those regions, before flowing through the jumper tube towards the manifold, where the pressure decreased from about 1000 Pa to the low hundreds of Pa within the manifold.

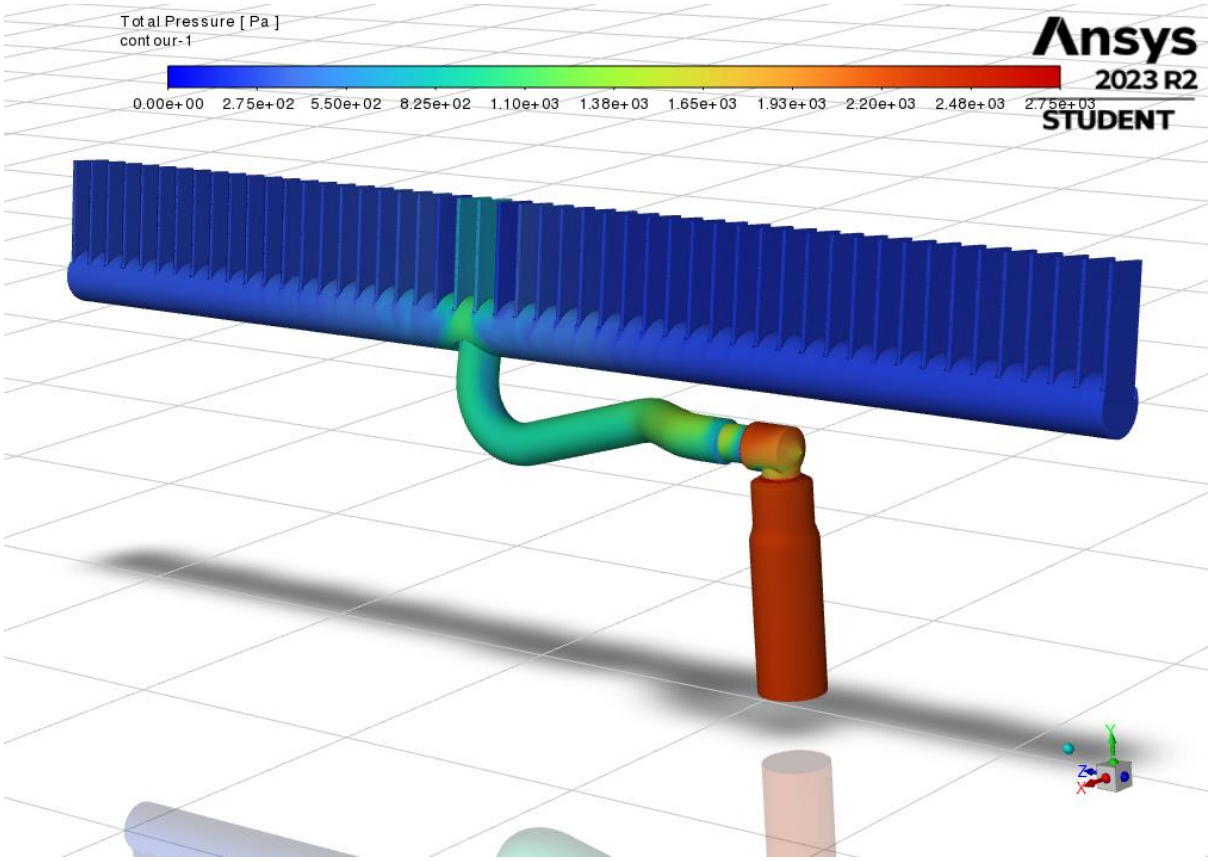

Figure 19 - Angled view of the total pressure distribution within the original design.

A different angle of the pressure contours shows that the bends and contraction in the jumper tube geometry resulted in drops in pressure, with the highest pressure in the manifold being in the channels directly above the point of inflow into the manifold.

The view from the back of the mesh allows to see that the total pressure within the manifold wanes quite substantially over a short distance (almost 1000 Pa over about 25mm).

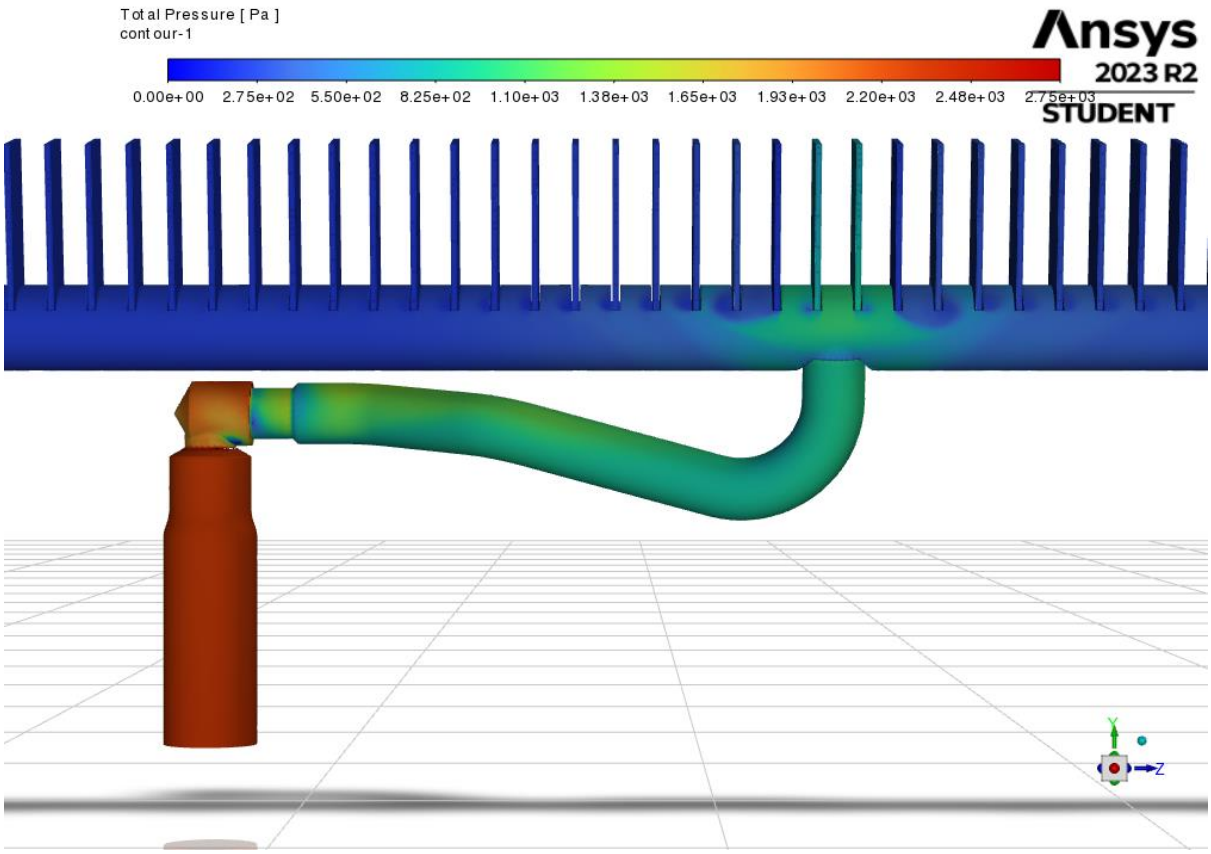

Figure 20 - Back view of the total pressure distribution within the original design.

In fact, the particle pathlines show that flow rapidly loses velocity as it becomes trapped in vortices created between the individual channels.

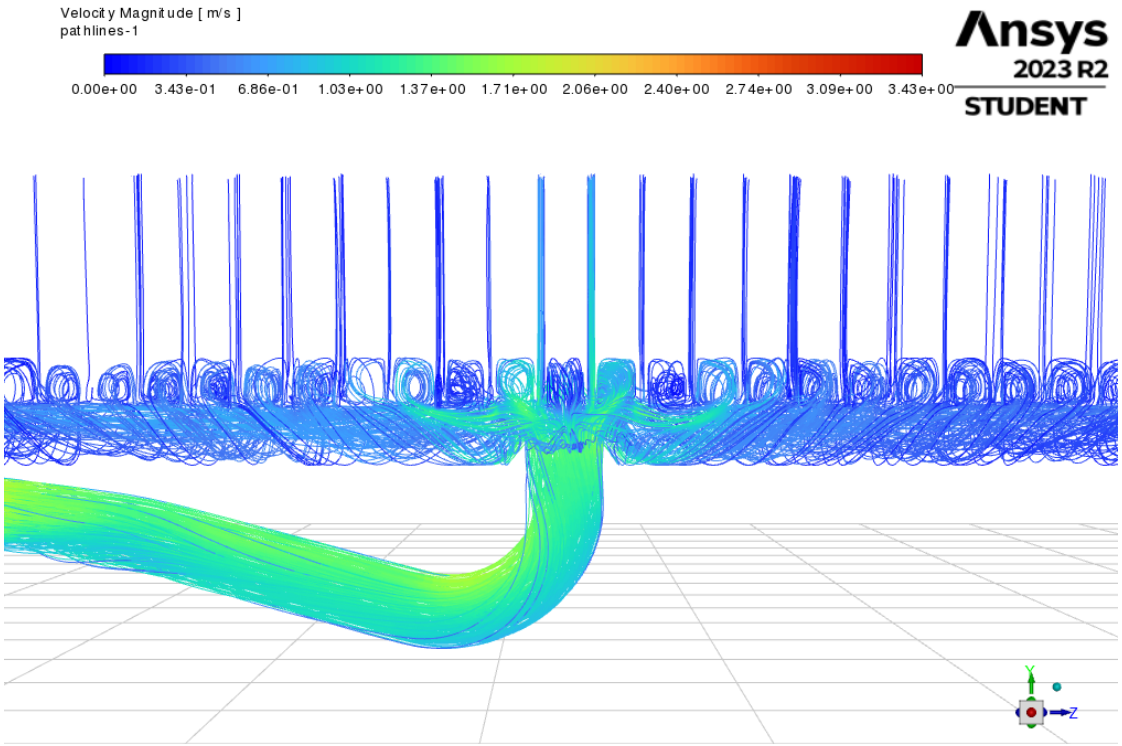

Figure 21 - Particle velocity pathlines within the original design.

The monitor for the mass flow rate passing through each outlet allows to visualize the distribution of flow in the manifold. The negative values indicate that flow is exiting the model.

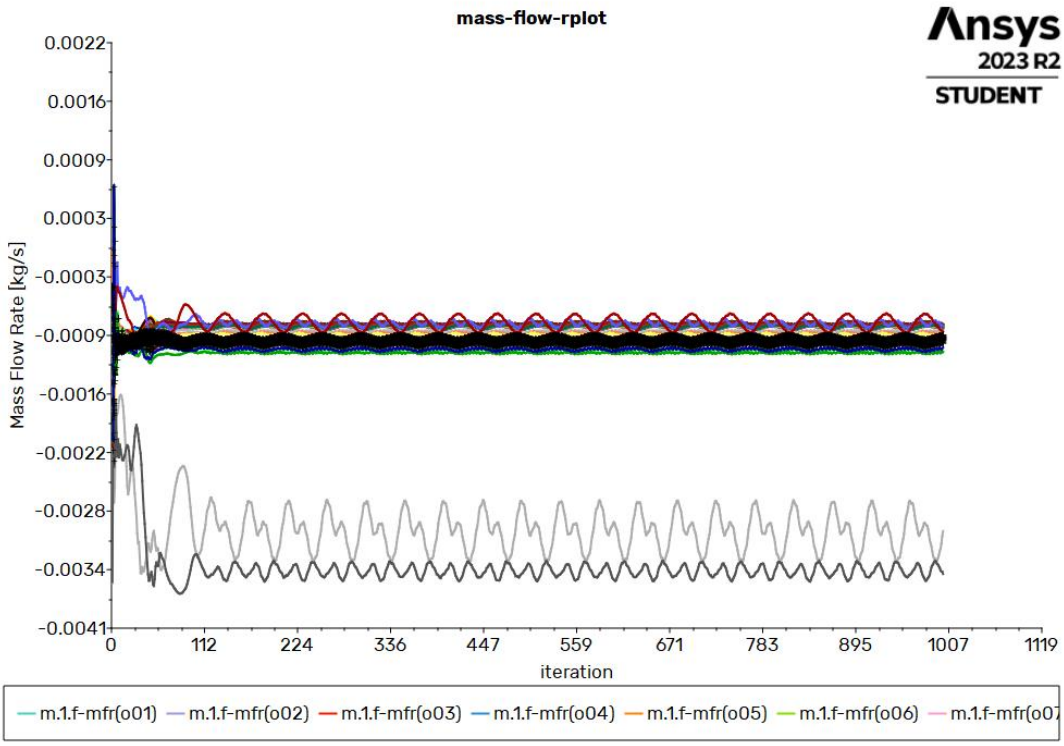

Figure 22 - Mass flow rate passing through each outlet of the original design, over 1000 iterations.

The black and grey lines at the bottom of the graph, with the highest mass flow rate values, represent the outlets situated directly above the inlet into the manifold. The flow is directed directly into them, reducing the amount of refrigerant supplied to the rest of the outlets. This distribution can be better visualized with a bar chart of absolute mean mass flow rate per outlet per 1000 iterations situated above each corresponding outlet.

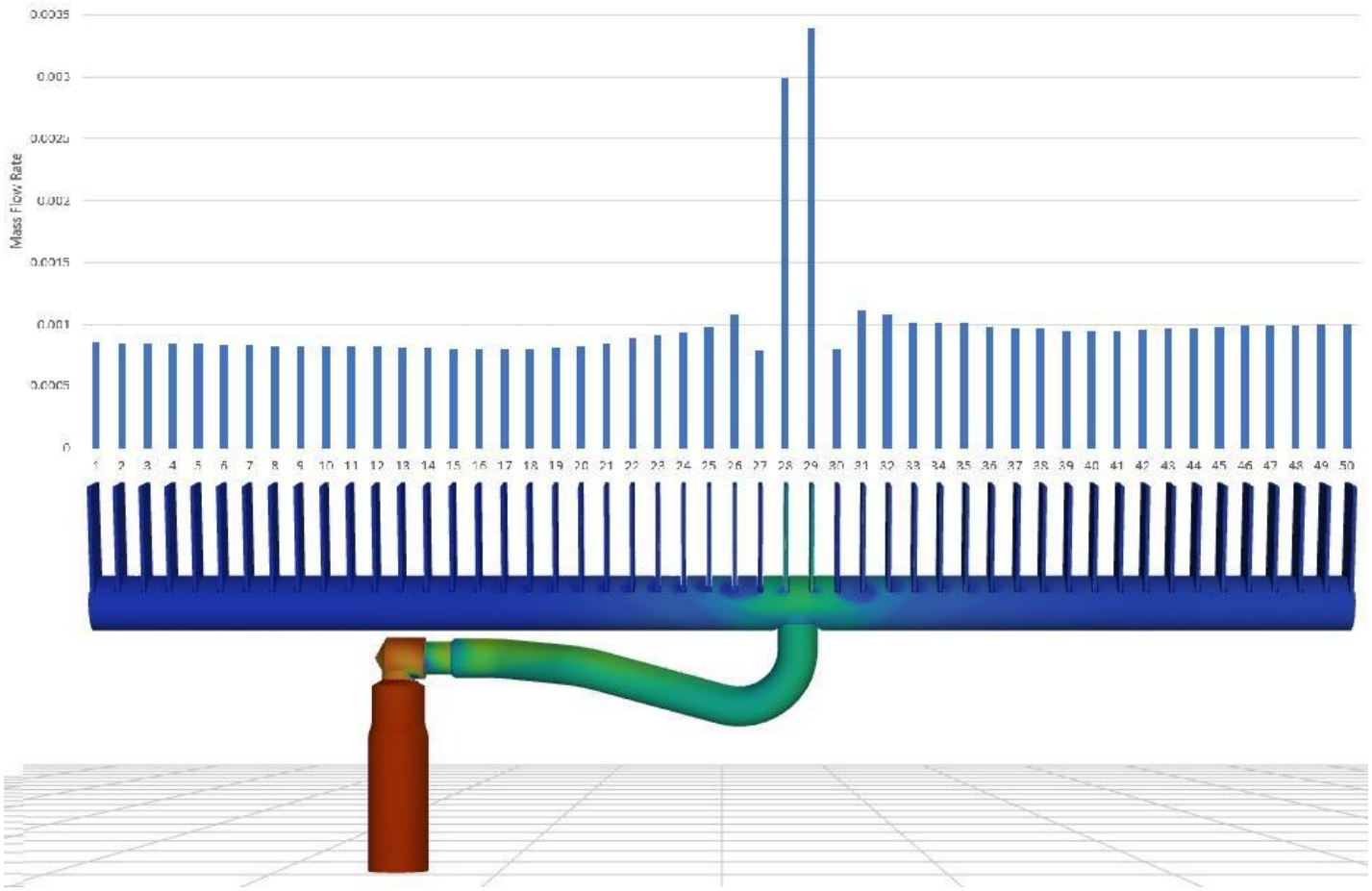

Figure 23 – Mean mass flow rate per outlet per 1000 iterations in each outlet corresponding to the channels in the original model.

The high mass flow rate in channels situated above the inlet to the manifold partially starves the channels directly adjacent to them of flow, resulting in the decreased flow in nearby tubes. The mass flow then gradually decreases, until eventually levelling out. The leftmost tubes in the channel (tubes 1-6) have slightly higher mass flow rate, although only marginally so. This can be explained by the gravitational effects acting on the model.

The second design can then be analysed.

Residuals of the second design have likewise not decreased as much as expected, due to the poor initial guess. The residuals show signs of stability, indicating convergence

has been achieved.

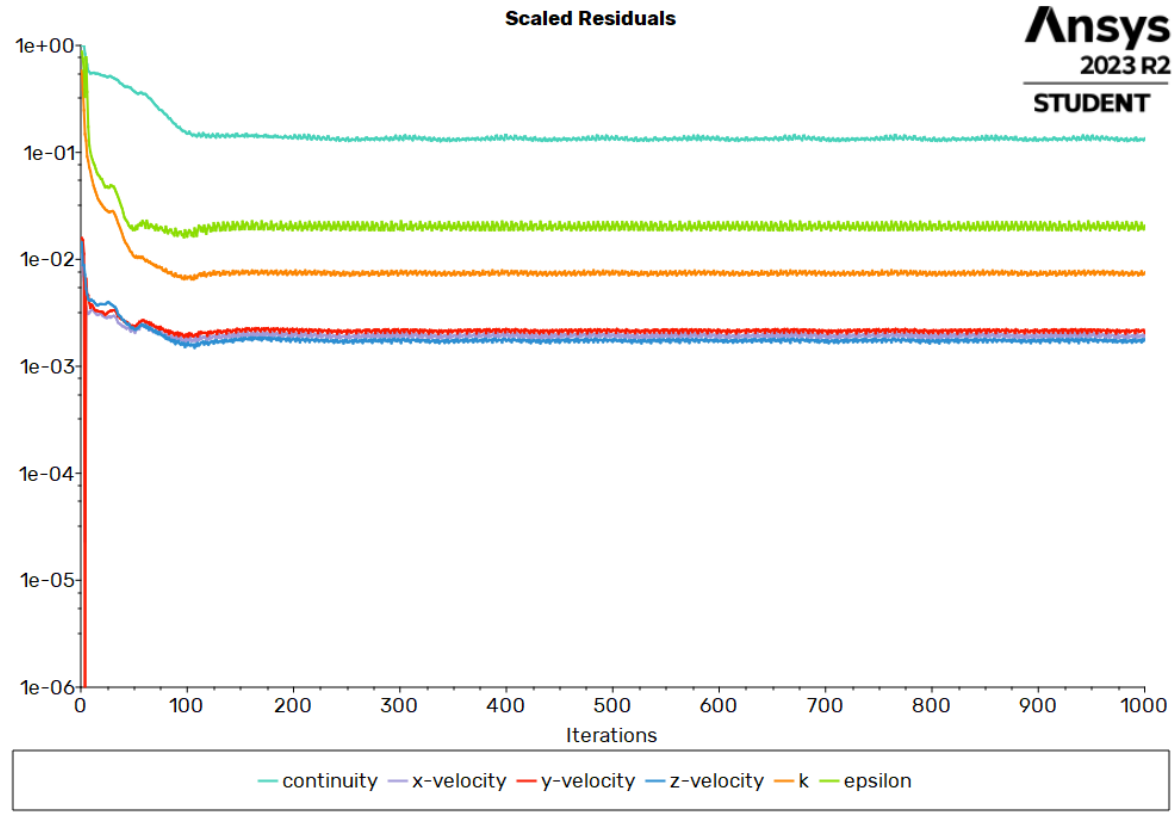

Figure 24 - Residuals of the simulation of the second design, over 1000 iterations.

The total pressure at the inlet confirms that convergence of the solution has in fact been reached.

The total pressure at the inlet for this design is shown to be smaller than in the original design. Since the boundary conditions are identical, this can only be attributed to the geometry. The total pressure at the inlet after convergence was 2134,99 ± 13,39Pa.

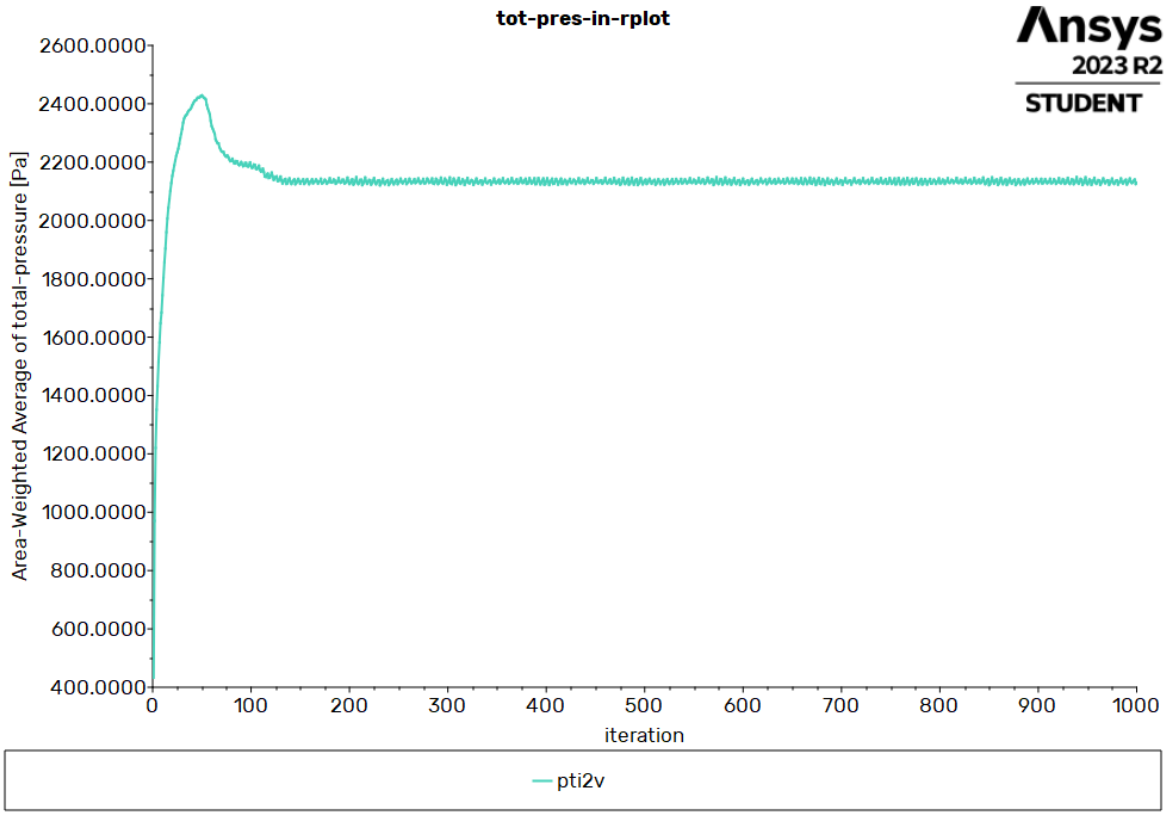

Figure 25 - Total inlet pressure for the second design, over 1000 iterations.

The total pressure distribution at the outlets produced the following graphical result:

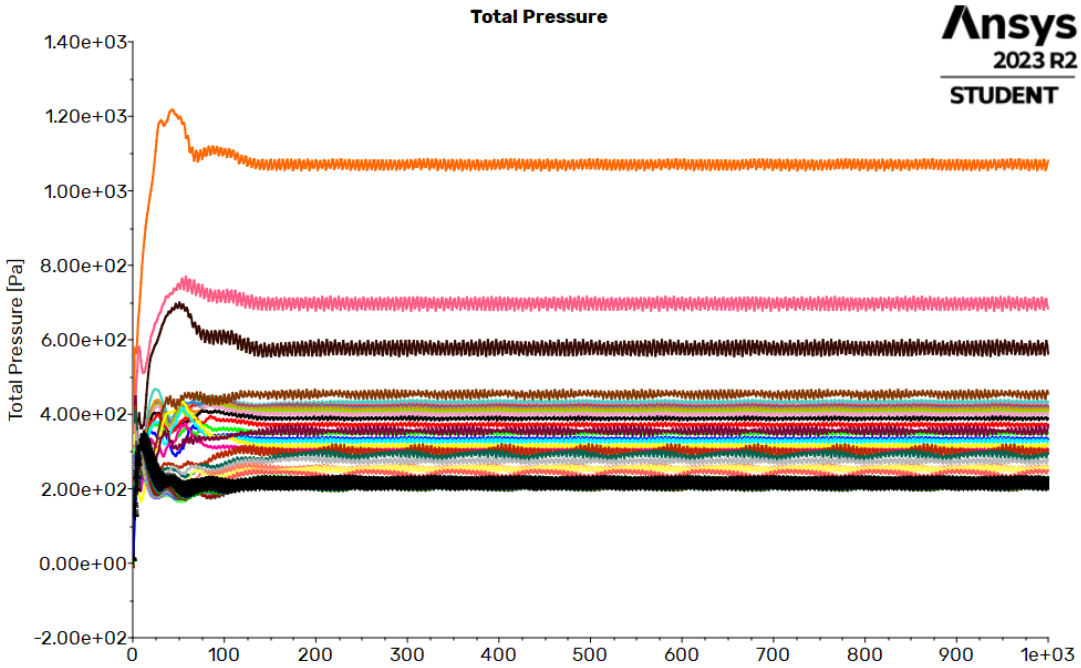

Figure 26 - Total pressure for each outlet of the second design, over 1000 iterations.

The highest pressures, just as in the original design, were recorded for the outlets directly above the inlet to the manifold. The average total pressure for all the outlets was close to that of the original design, measuring at 308,55 ± 0,52 Pa.

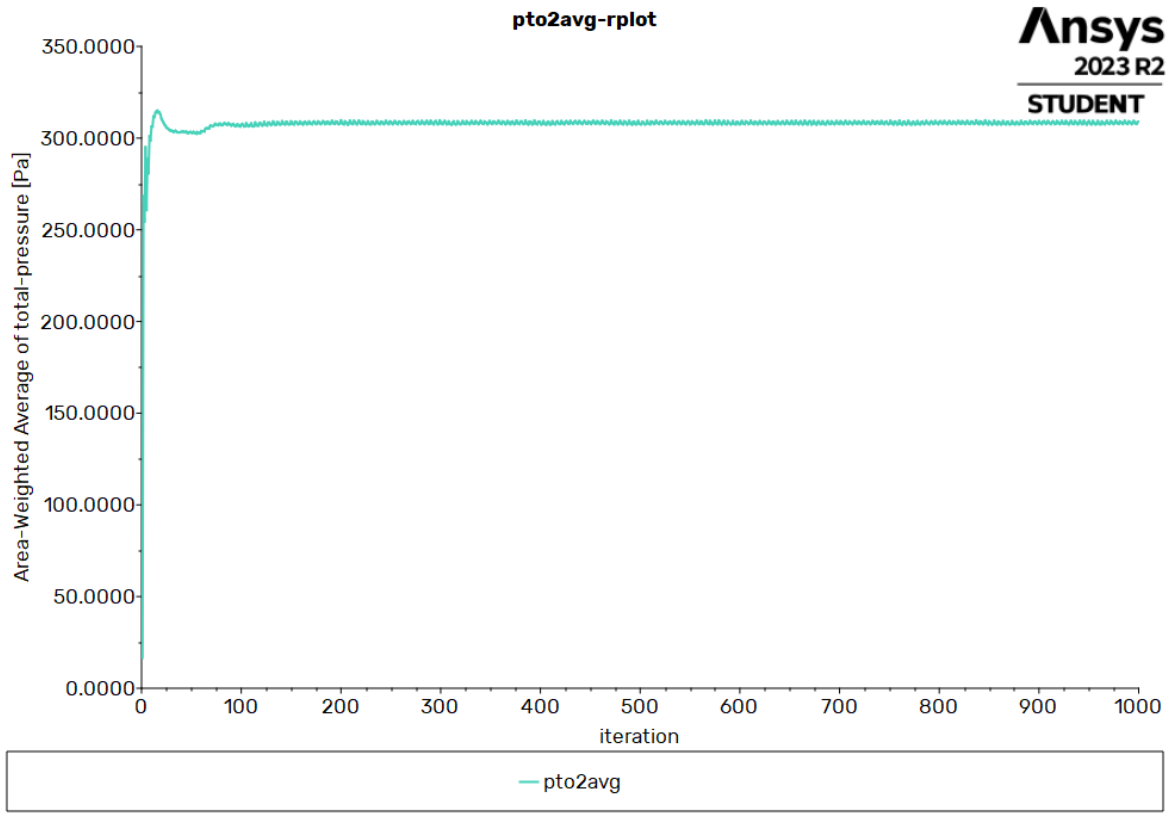

Figure 27 - Mean total outlet pressure of the second design, over 1000 iterations.

The average pressure drop Δp within this design can therefore be calculated to be: $\Delta p_{avg} = p_{in} - p_{outavg}$ = 1826,44 ± 13,92 Pa.

The total pressure contours show the pressure being highest in the manifold and in the channels directly above the inlet.

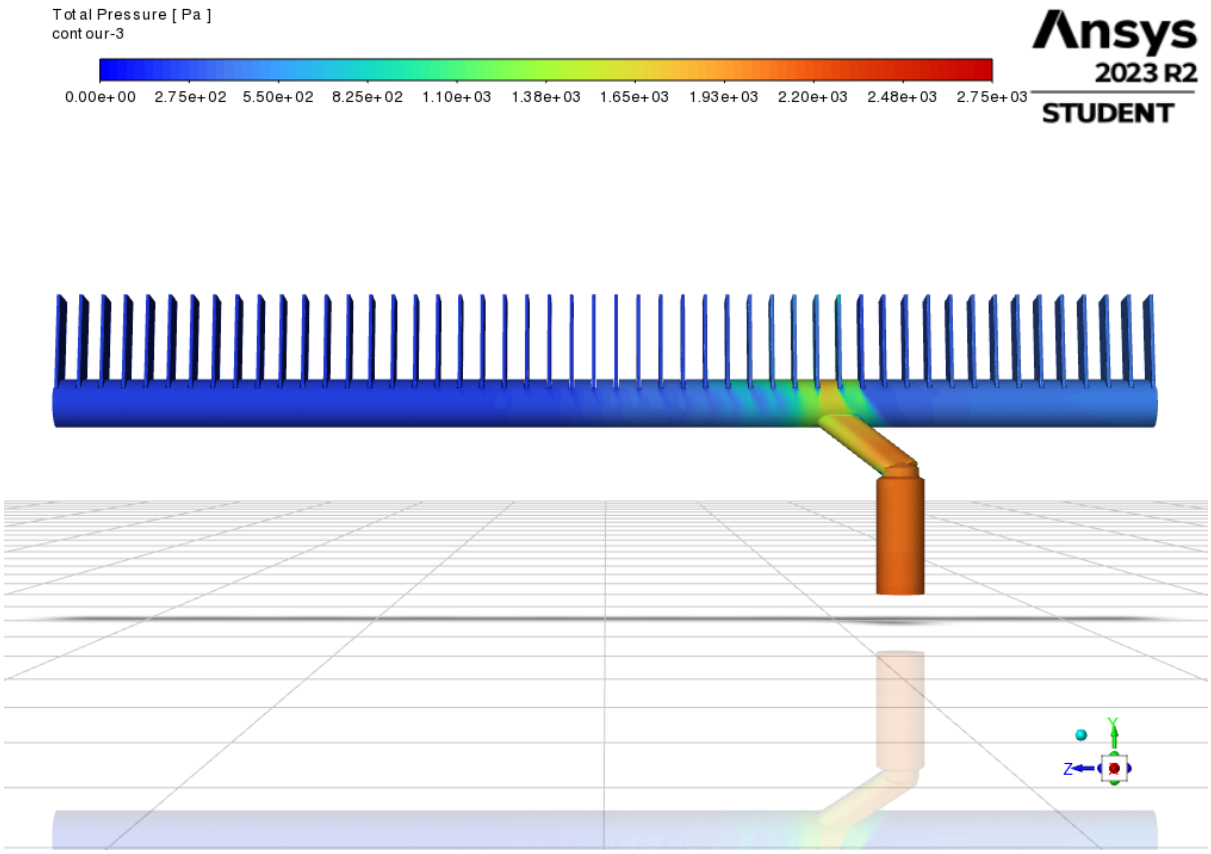

Figure 28 - Frontal view of total pressure distribution within the second design.

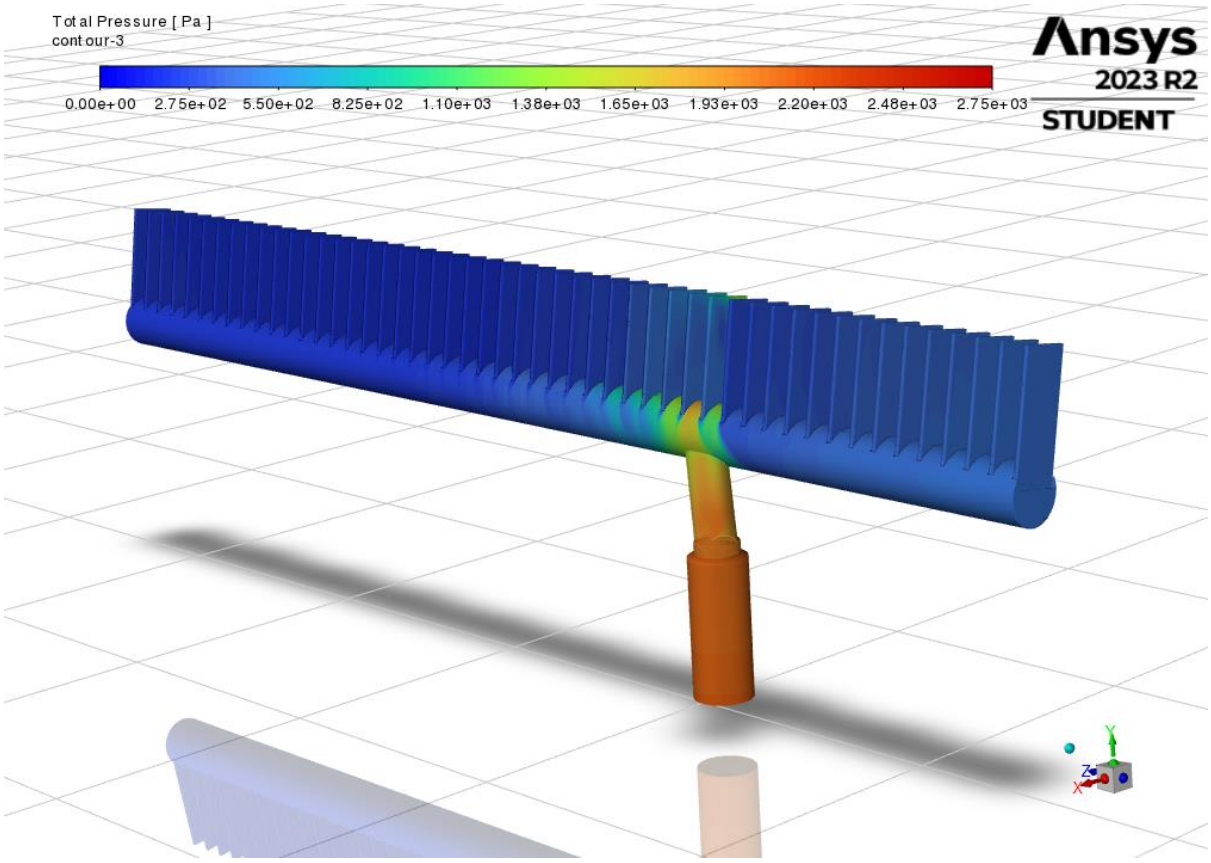

Figure 29 - Angled view of the pressure distribution within the second design.

The pressure seems to drop in the left-hand side of the manifold quicker due to the formation of vortices on the upper walls between the channels. This occurs, as in the original design, due to vortex formation on the walls between the channels, with flow losing energy quickly as it expands towards the end of the manifold. From the particle pathline diagrams it is possible to see that the left-hand side, or “upper” part of the manifold (with respect to orientation in the vehicle), is prone to generating more numerous and larger vortices.

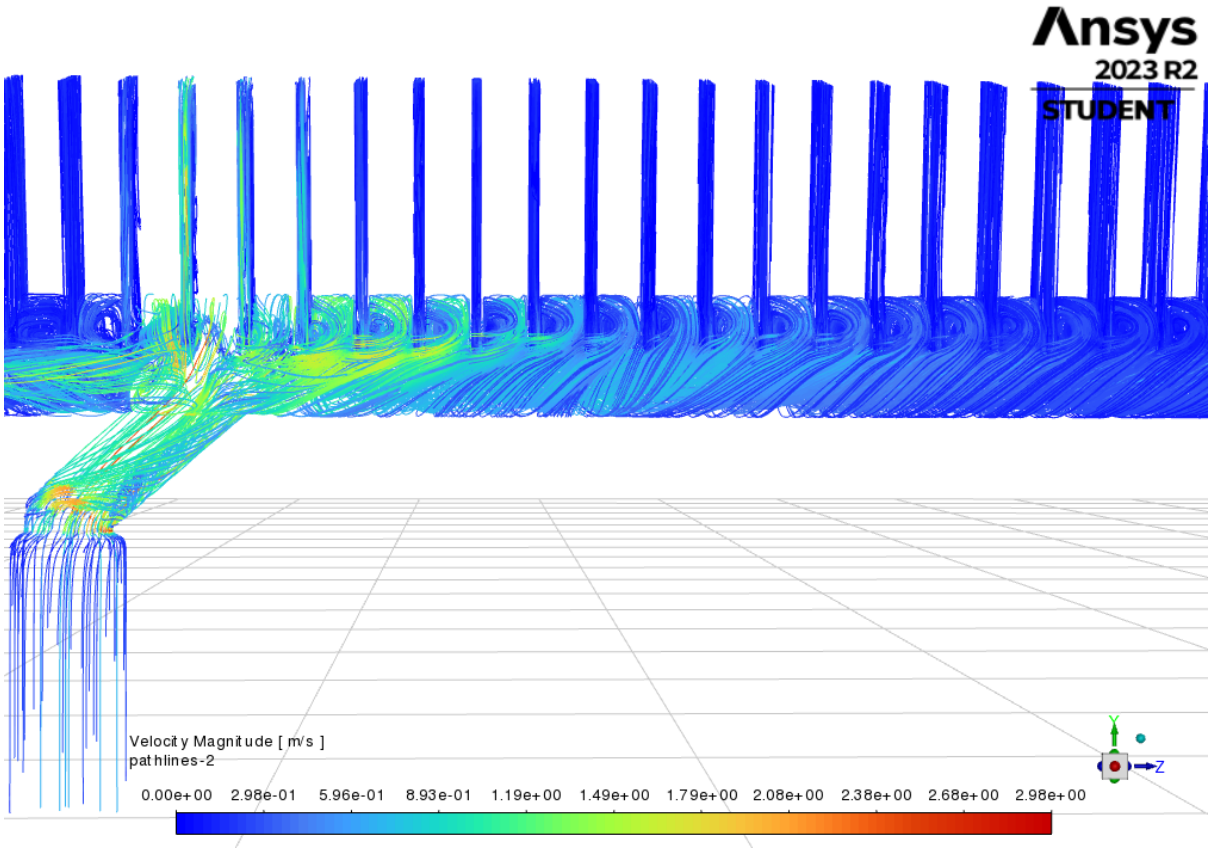

Figure 30 - Pathline diagrams showing the back view of the second design manifold, with clearly noticeable vortices between the channels.

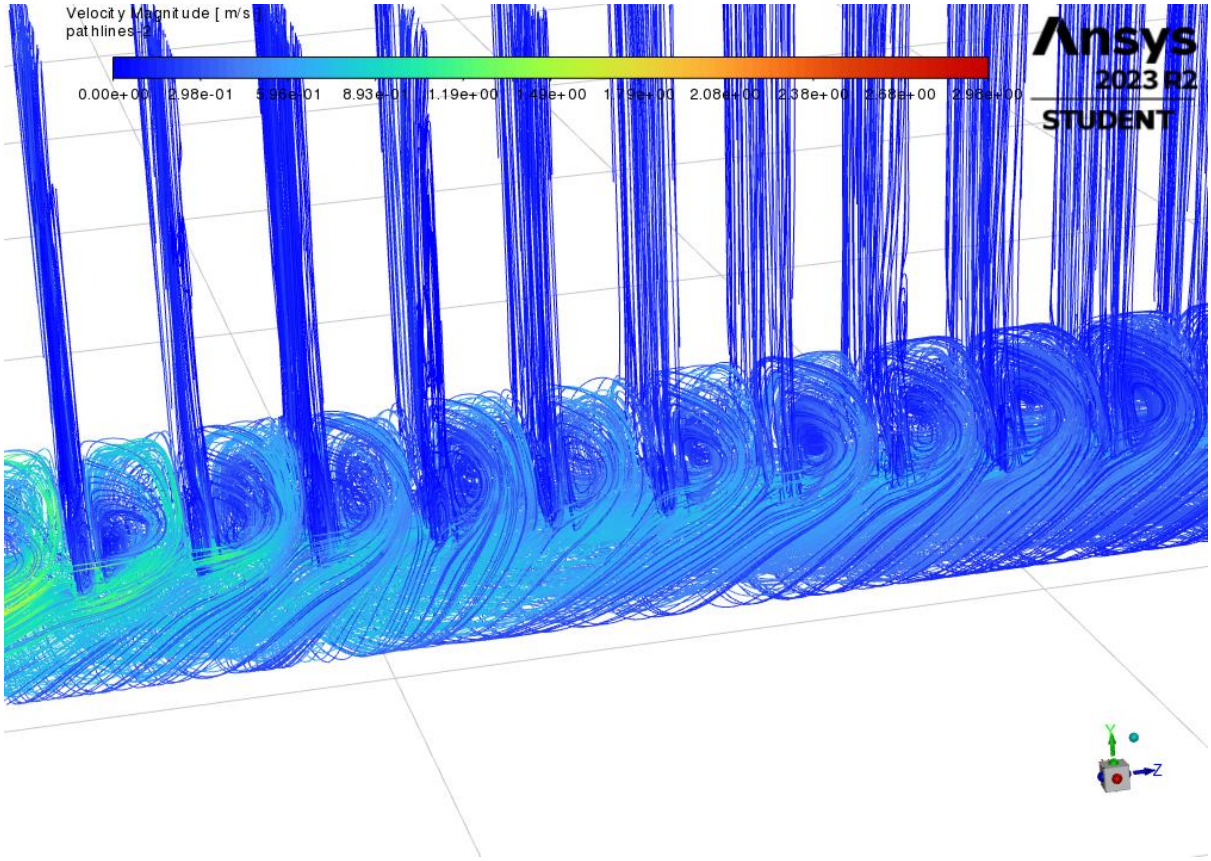

Figure 31 - Closer view of the formed vortices in the second design.

The mass flow rate monitor once again showed the highest mass flow rate being recorded within the tubes directly above the inlet:

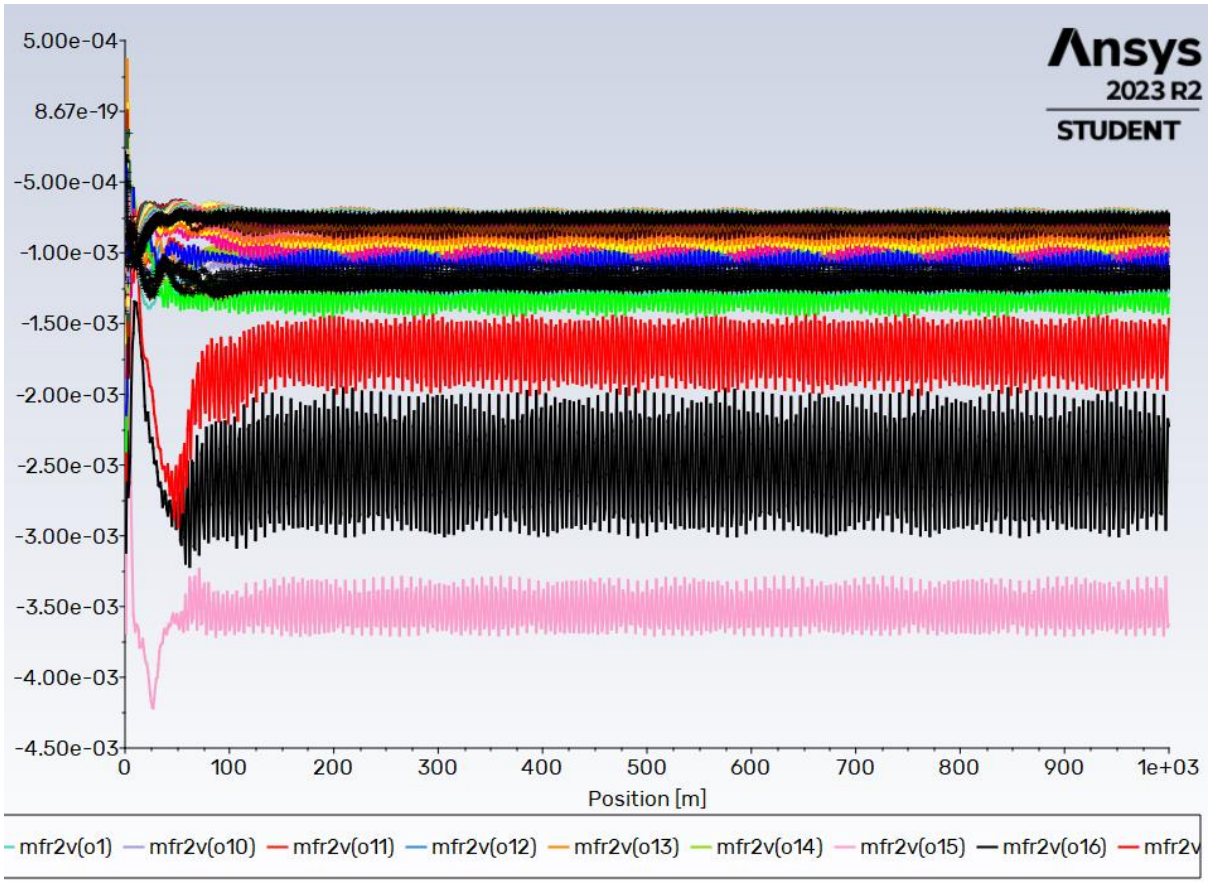

Figure 32 - Mass flow rate graph for each outlet within the second design, over 1000 iterations.

The lines with the highest mass flow rates correspond to channels number 15, 16, 17 and 18, in order of decreasing mass flow rate magnitude. Plotting a bar chart of absolute mean mass flow rate per outlet over 1000 iterations corresponding to each numbered outlet further shows the disproportionately large mass flow rate in tubes above the inlet port.

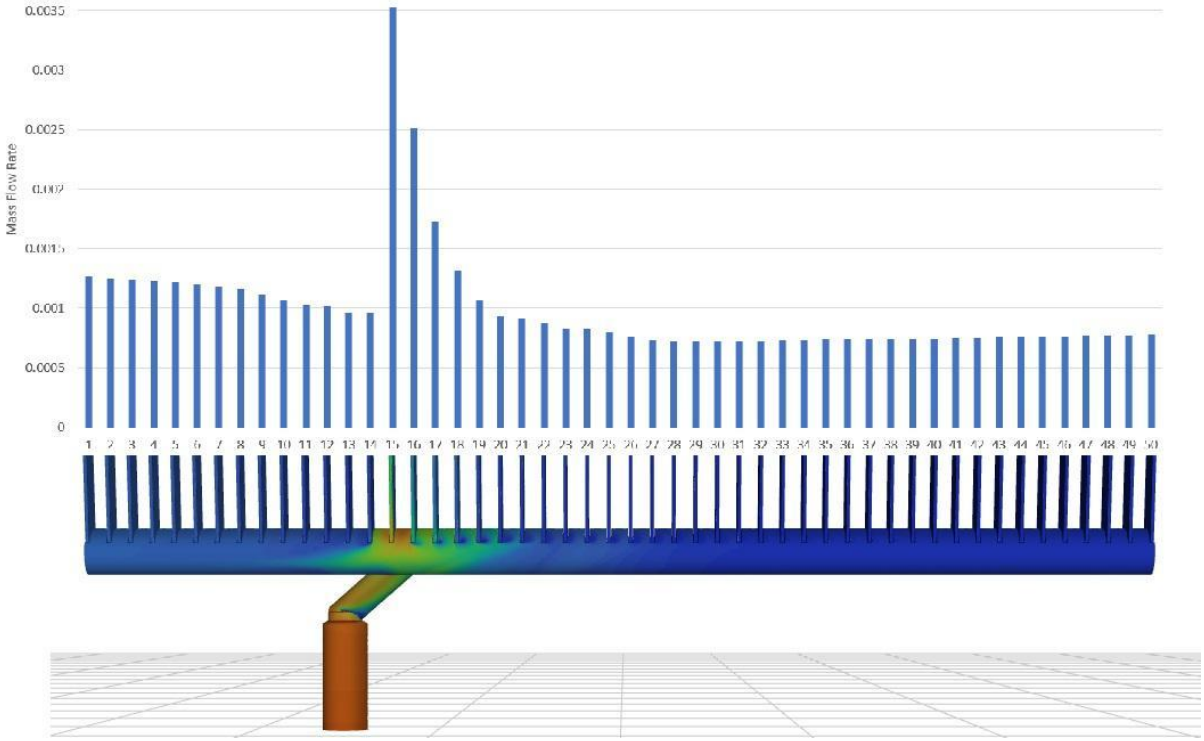

Figure 33 – Mean mass flow rate per outlet per 1000 iterations in each outlet with the corresponding channels of the second design.

The heightened mass flow rate in tubes 1-10 corresponds to the gravitational effects acting on the refrigerant. The geometry, just as in the original design causes the flow to be unevenly distributed.

On the basis of these findings, the suggested design produced by the student incorporates an inflow channel that supplies the manifold perpendicularly to the outlet channels (Figures 6 and 7). This was done in order to theoretically minimize the maldistribution of flow, due to it being mostly captured by outlet channels directly adjacent to the point of inflow.

Residual plots show that the solution residual have decreased to the same approximate levels as in the previous simulations, and have stabilized, suggesting convergence was reached.

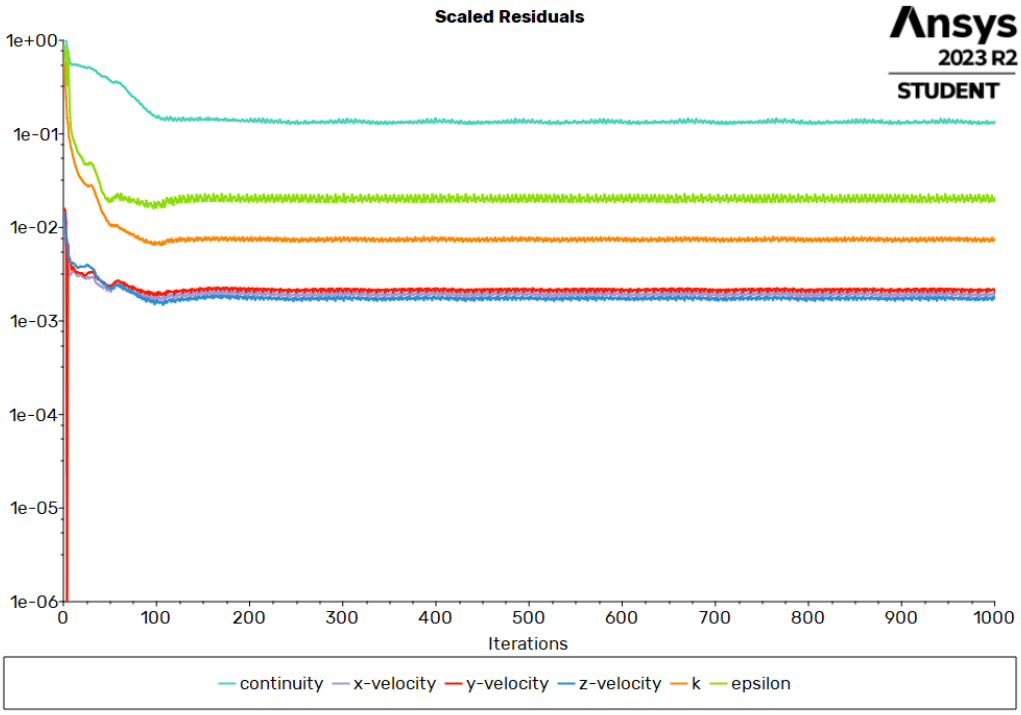

Figure 34 - Residuals of the suggested design, over 1000 iterations.

The total pressure monitored at the inlet further shows that convergence has been reached and shows a reduction in pressure when compared to the previous two designs.

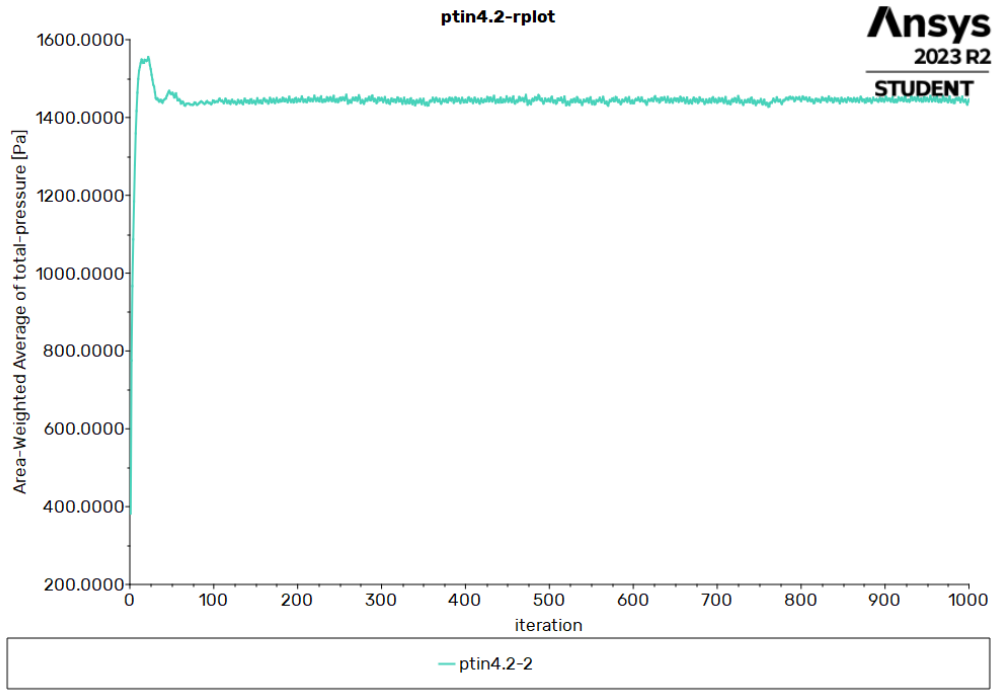

Figure 35 - Monitor of the inlet pressure of the suggested design, over 1000 iterations.

The total pressure at the inlet was measured to be 1444,40 ± 11,98 Pa.

The total pressure at the outlets shows that some outlets have higher pressure than the rest. In this case, however, the outlets with the highest pressure are those that are located to the right of the inlet, not above, as in the previous designs.

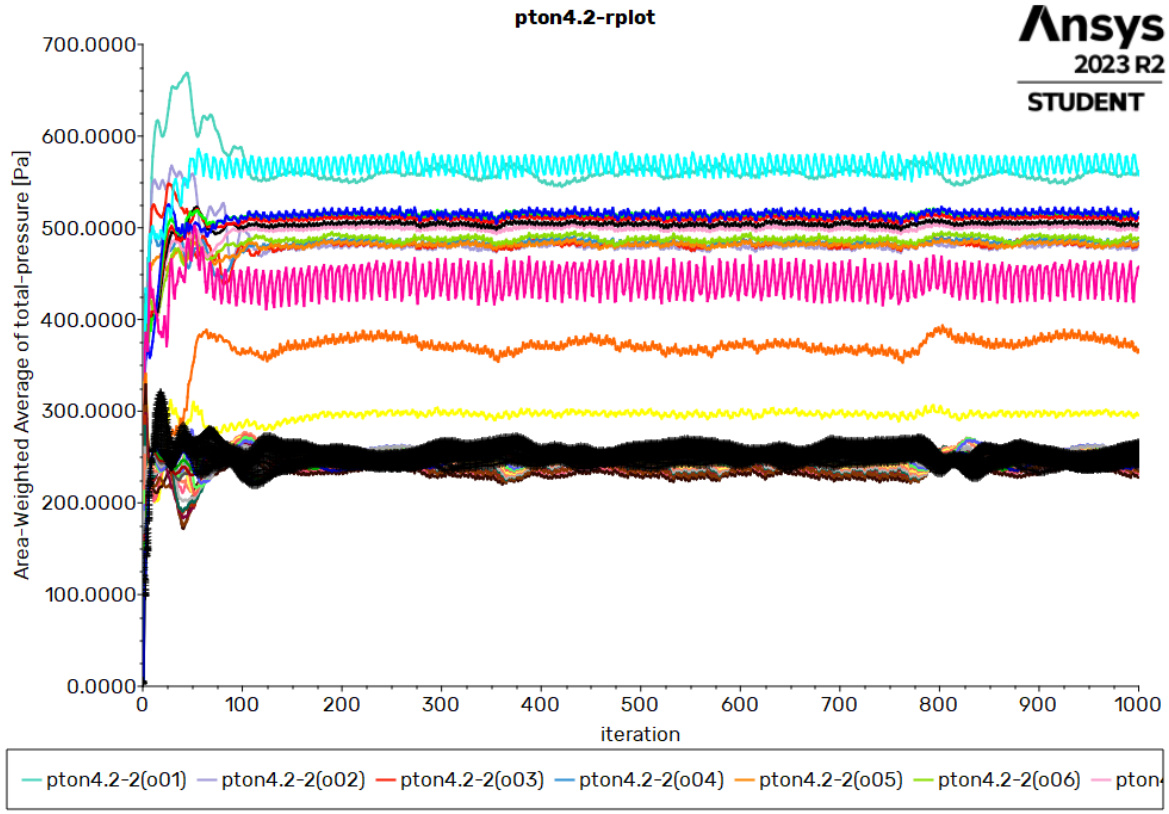

Figure 36 - Monitor of total pressure at each of the outlets of the suggested design, over 1000 iterations.

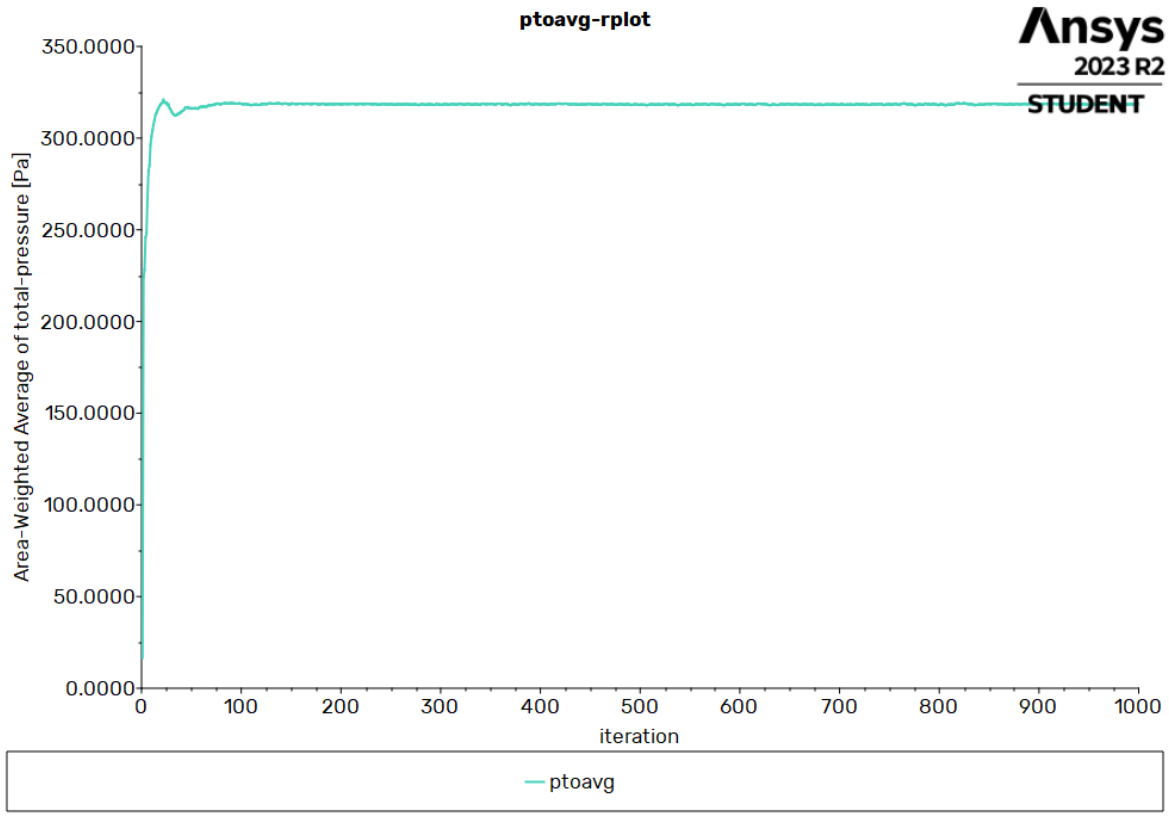

Figure 37 - Average total pressure for all outlets of the suggested design over 1000 iterations.

The average total pressure at the outlet was measured to be 318,42 ± 0,21 Pa.

From these measured values, pressure drop can be calculated:

$$\Delta p_{avg} = p_{in} - p_{outavg} = 1125{,}98 \pm 6{,}095 \text{ Pa}$$

The increased pressure within the rightmost channels can be clearly seen from the pressure contours:

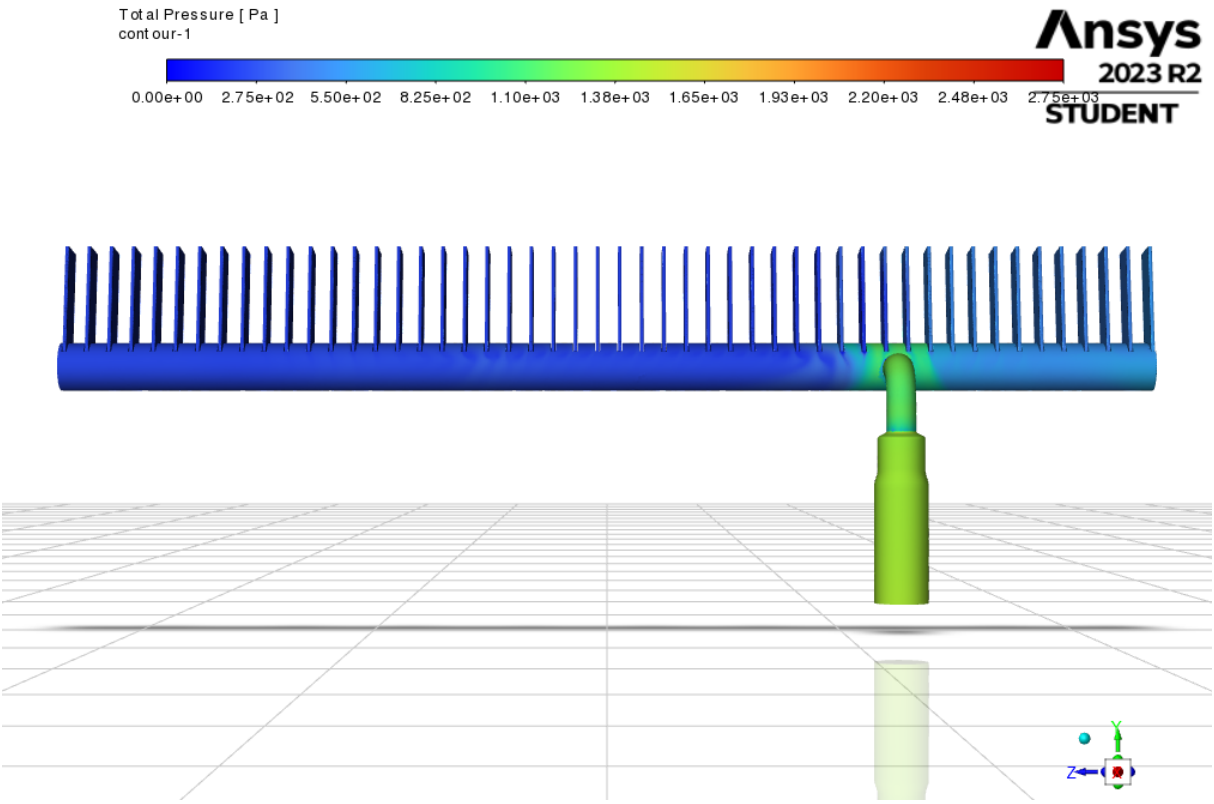

Figure 38 - Frontal view of the total pressure distribution within the suggested design.

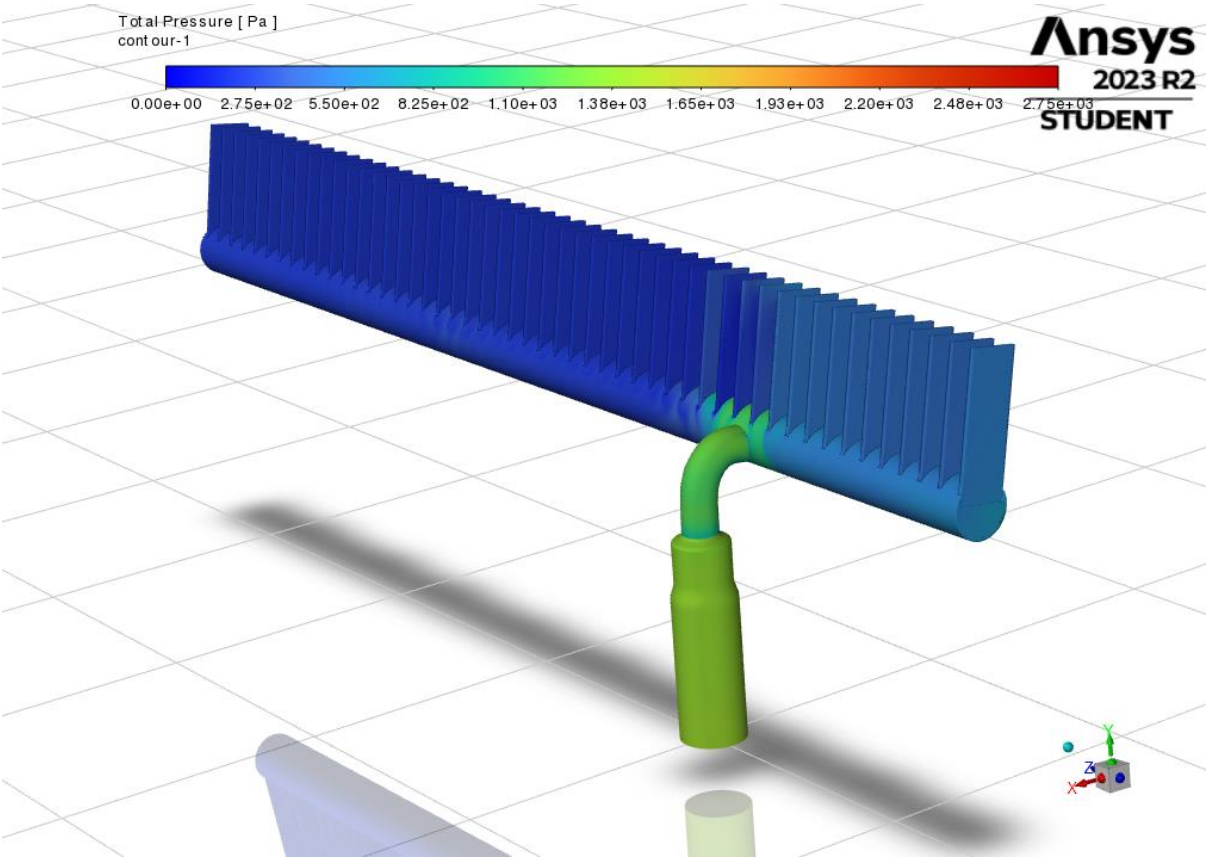

Figure 39 - Angled view of the total pressure distribution within the suggested design.

The pressure contours confirm that the pressure in channels 1-13 have almost 350 Pa more total pressure.

From the pathline diagrams it is possible to see that the left side of the manifold is particularly subjected to vortex formation, whereas the right is not affected by them to the same extent. Additionally, the gravitational forces seem to have a substantial effect on flow in this design.

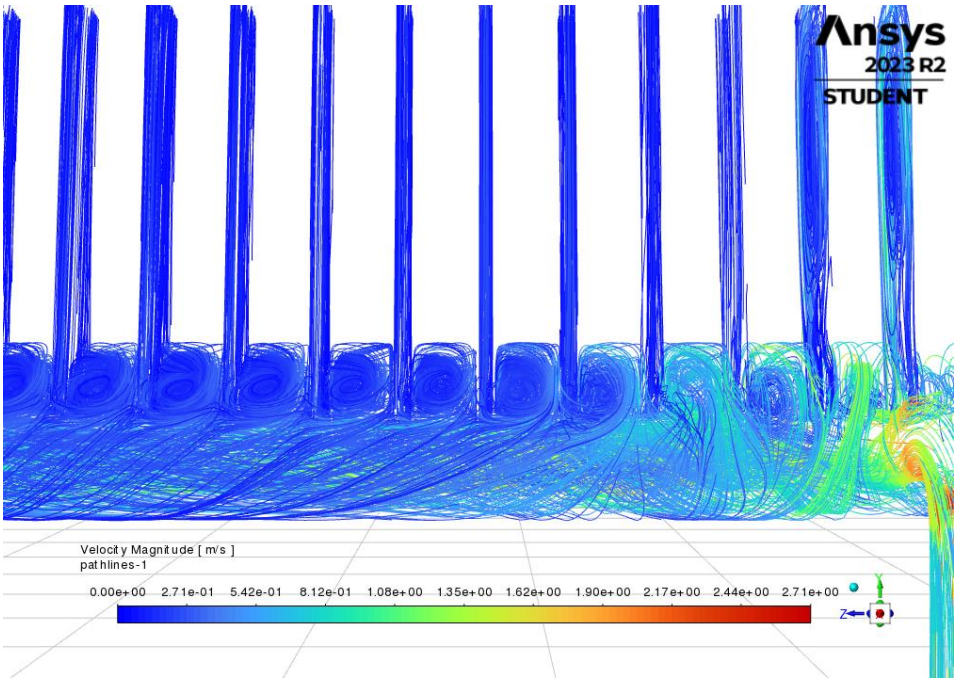

Figure 40 - Particle pathline diagram for the suggested design, to the left of the inlet.

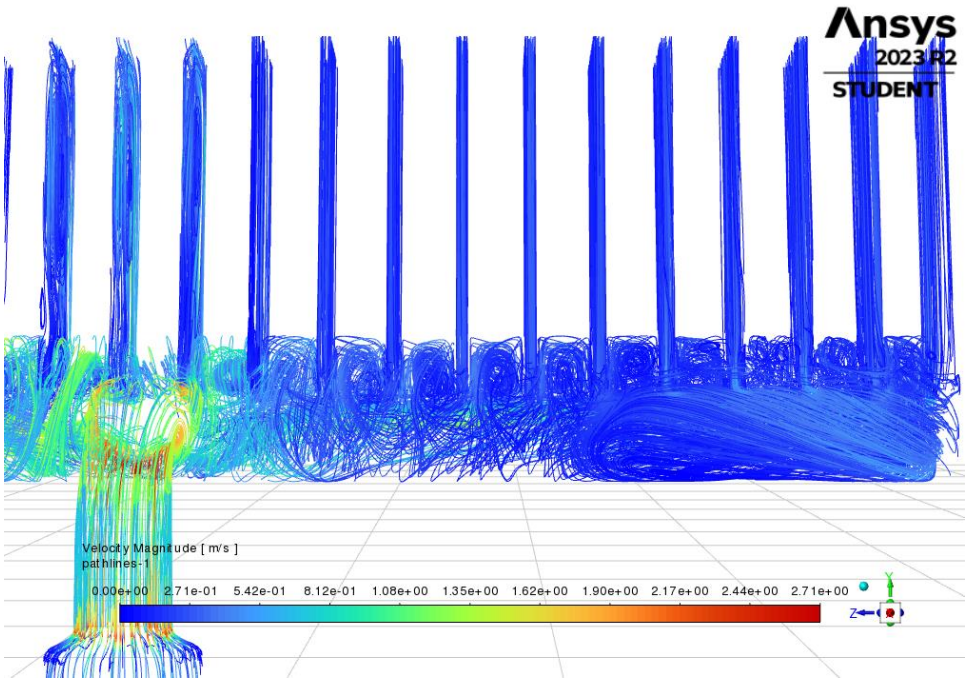

Figure 41 - Particle pathline diagram for the suggested design, to the right of the inlet.

From the back view, the pathlines show that flow collides with the wall of the manifold and bifurcates along the back wall, swirling between the channels and forming vortices.

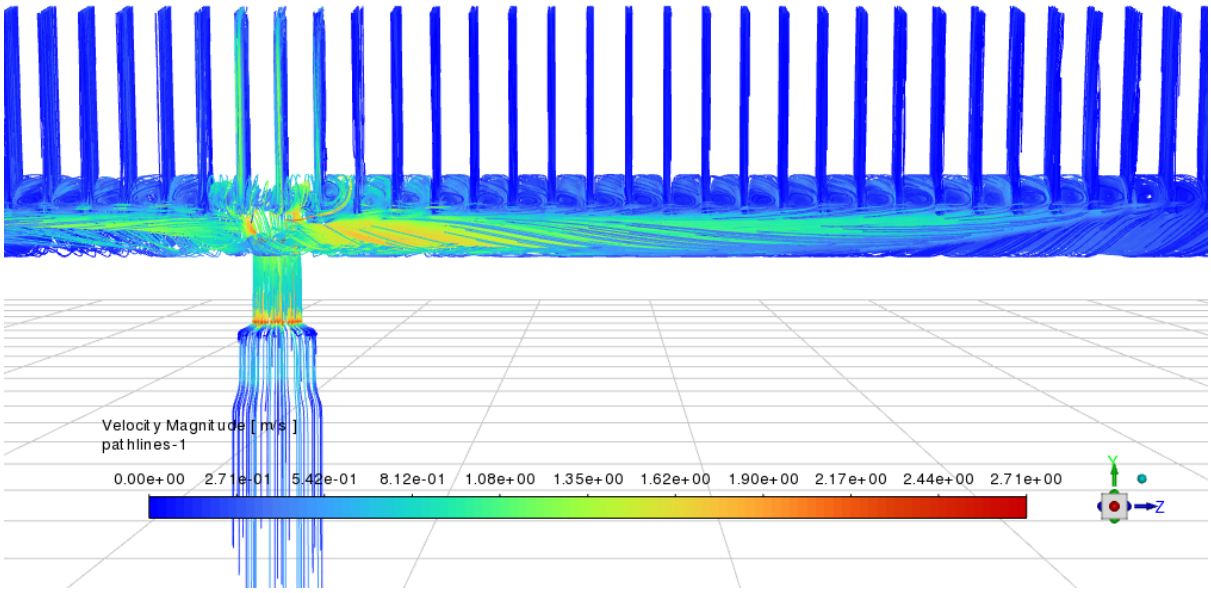

Figure 42 - Particle pathline diagram for the suggested design, as viewed from the back.

The mass flow diagram shows that some channels, as in previous designs, have higher mass flow rate than the rest. However, the difference is not as substantial as in the other models. The highest mass flow rates occur in the part of the manifold that would, in practice, be closest to the ground. The highest mass flow rate occurs in channel 1.

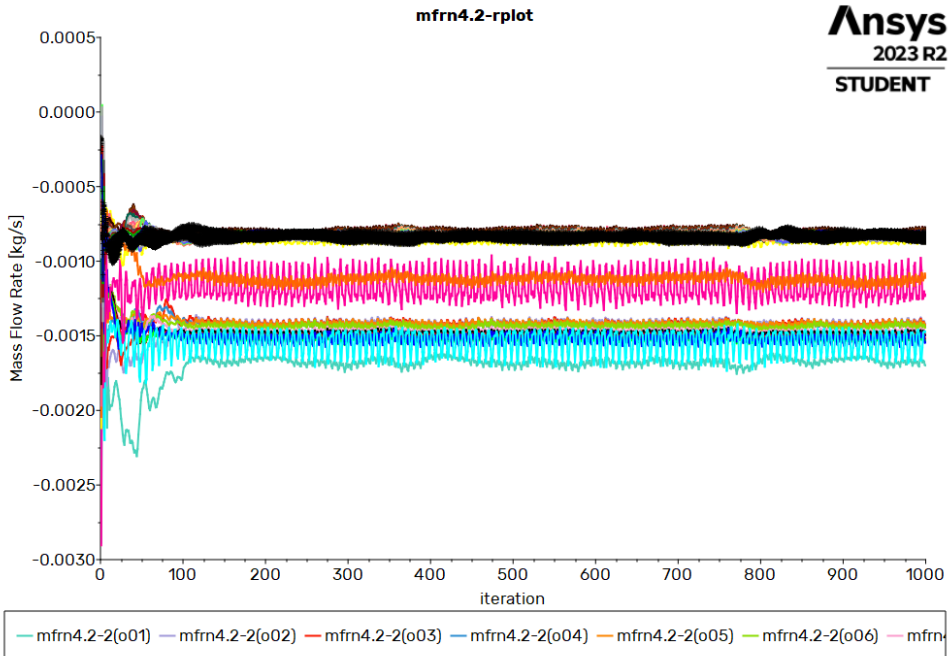

Figure 43 - Mass flow rate distribution in each outlet within the suggested design over 1000 iterations.

In the bar chart diagram of mean mass flow rates per outlet per 1000 iterations these higher mass flow rates are even more apparent.

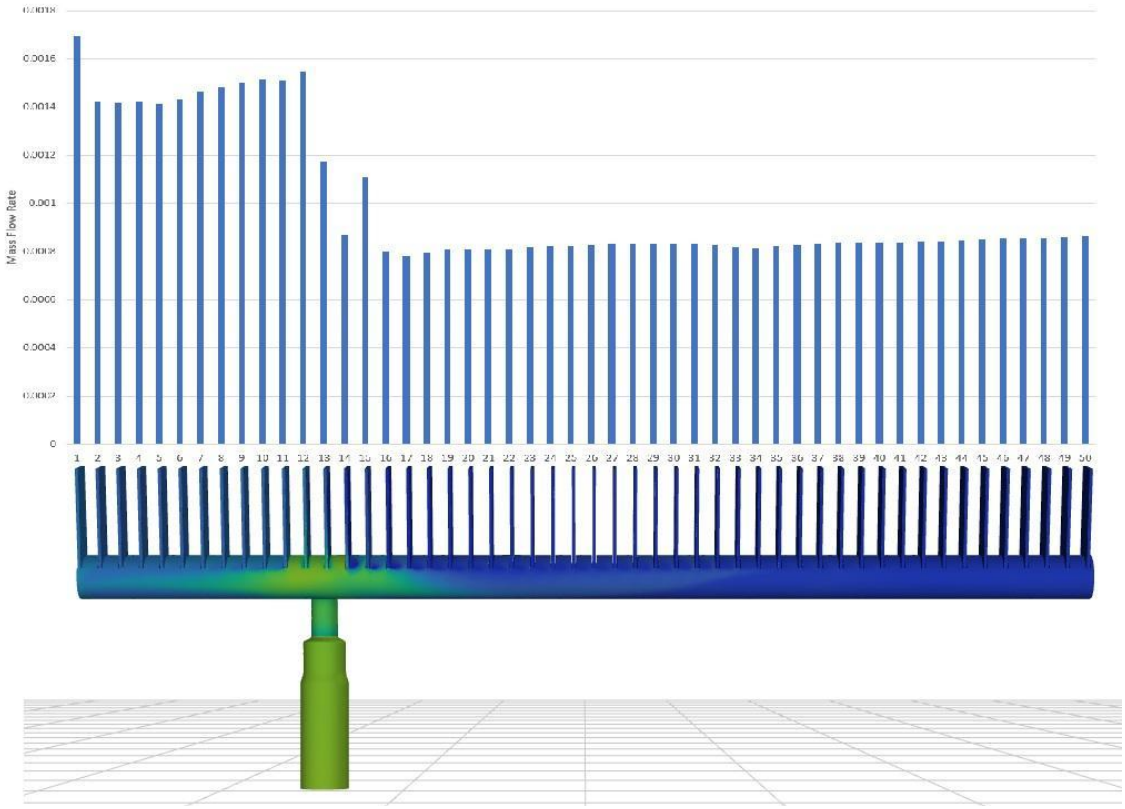

Figure 44 - Average mass flow rate for each outlet with the corresponding channels in the suggested design.

The most important parameters that were monitored over the course of the simulations – the pressure drop and mass flow rate distribution – are both lower than those measured in the first and second designs.

The overall reduction in pressure drop in the suggested design is 45,7% when compared to the original design, and 38,3% when compared to the second. Plotting all the mean mass flow rate distributions onto one graph shows that the overall distribution of flow is more even, and the difference in maximum and minimum values is lower in the suggested design.

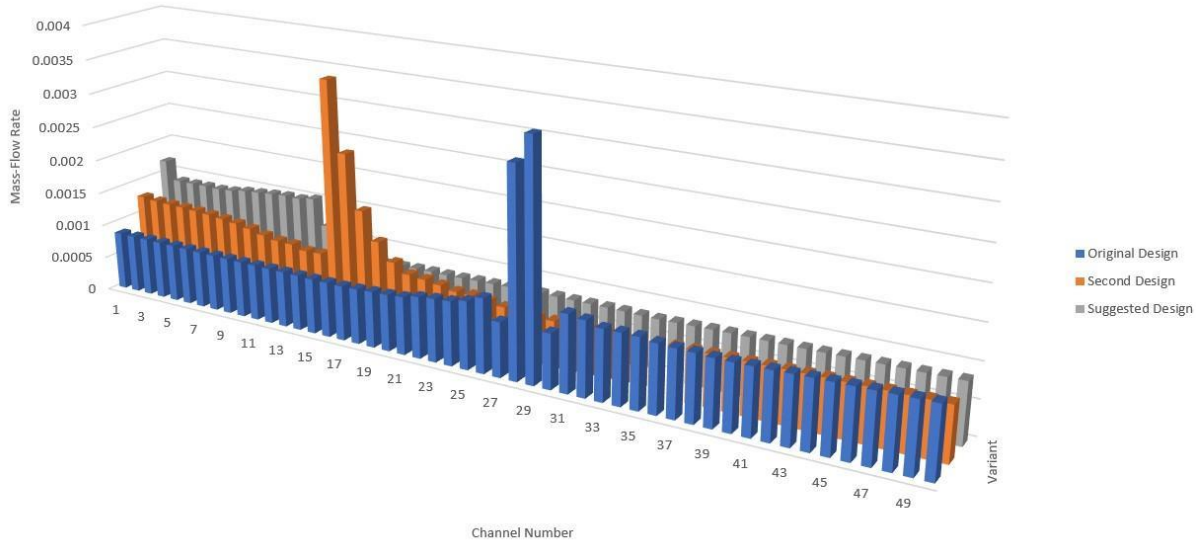

Figure 45 - Comparative bar-chart of mean mass flow rate per outlet over 1000 iterations for all three designs.

The differences in maximum and minimum mean outlet mass flow rates for each outlet over 1000 iterations in each design are shown in the table below.

$\Delta\dot{m}$ [kg/h]	
Original Design	0,002605
Second Design	0,002804
Student-Suggested Design	0,000911

Figure 46 - Table of differences between highest and lowest mean mass flow rate per outlet over 1000 iterations for each design.

The reduction in mass flow rate difference is 65,02% when compared to the original design, and 67,51% when compared to the second design.

Conclusion

Three inlet manifolds and inlet geometries have been simulated using ANSYS Fluent and tested under the same initial conditions, accounting for the predicted pressure loss within the tubes of the real condenser. Mass flow rate graphs, as well as inlet, outlet and average total pressure graphs have been produced and analysed. Total pressure contours, pathline and mean mass flow distribution diagrams gave been produced and analysed. The results have shown that the suggested design developed for this thesis, when compared to the first and second designs, resulted in a reduction of the pressure drop by 45,7% and 38,3% respectively. The difference in mean mass flow magnitudes has likewise been calculated, resulting in a reduction of 65,02% and 67,51% respectively. The two goals of this thesis, to reduce pressure drop and maldistribution, have therefore been achieved. While there are opportunities for further improvements and optimizations, it is possible to conclude that the suggested design has fulfilled the necessary requirements and would in theory increase the performance of the condenser.

Bibliography

Ansys, Inc. (2023). *Fluent User's Guide* [Release 2023 R2]. https://ansyshelp.ansys.com/account/secured?returnurl=/Views/Secured/corp/v232/en/flu_ug/flu_ug.html

Bajura, R. A., Jones, E. H. (1976). Flow Distribution Manifolds. *Journal of Fluids Engineering*, *98*(4)

Brix, W., Kærn, M. R., Elmegaard, B. (2009). Modelling refrigerant distribution in microchannel evaporators. *International Journal of Refrigeration*, *32*(7)

Byun, H., Kim, N. (2011). Refrigerant distribution in a parallel flow heat exchanger having vertical headers and heated horizontal tubes. *Experimental Thermal and Fluid Science*, *35*(6)

Choi, J. M., Payne, V., Domanski, P. A. (2003, August 17-22). *Effects of Non-Uniform Refrigerant and Air Flow Distributions on Finned Tube Evaporator Performance*. Refrigeration International Congress, 21st IIR. (IRC2003). 10th Technical Session Energy-Efficient Heating and Cooling Systems for Buildings, Washington, DC, USA.

Choi, S. H., Shin, S., Cho, Y. I. (1993). The effect of area ratio on the flow distribution in liquid cooling module manifolds for electronic packaging. *International Communications in Heat and Mass Transfer*, *20*(2).

Chung, K., Lee, K-S., Kim, W- S. (2002). Optimization of the design factors for thermal performance of a parallel-flow heat exchanger. *International Journal of Heat and Mass Transfer*, *45*(24).

Datta, S., Das, P., Mukhopadhyay, S. (2016). Performance of a condenser of an automotive air conditioner with maldistribution of inlet air—Simulation studies and its experimental validation. *International Journal of Heat and Mass Transfer*, *98*.

Habib, M., Ben-Mansour, R., Said, S., Al-Qahtani, M., Al-Bagawi, J., Al-Mansour, K. (2009). Evaluation of flow maldistribution in air-cooled heat exchangers. *Computers & Fluids*, *38*(3).

Honeywell Inc. *HFO-1234yf - Thermodynamic Properties – IP units*. https://www.rsd.net/fx/pdf/suite/honeywell_genetron/Genetron_HFO-1234YF_PT_Chart.pdf

Honeywell Refrigerants Inc. (2015, May). *Solstice® yf Properties and Materials Compatibilit*y. https://www.honeywell-refrigerants.com/europe/wp-content/uploads/2015/06/Solstice-yf-Properties-and-Materials-Capatibility-060115.pdf

Huang, L., Lee, M. S., Saleh, K., Aute, V., Radermacher, R. (2014). A computational fluid dynamics and effectiveness-NTU based co-simulation approach for flow mal-distribution analysis in microchannel heat exchanger headers*. Applied Thermal Engineering*, *65*(1-2).

Huber, M. L., Assael, M. J. (2016, November). Correlations for the viscosity of 2,3,3,3-tetrafluoroprop-1-ene (R1234yf) and trans-1,3,3,3-tetrafluoropropene (R1234ze(E)). *International Journal of Refrigeration*, *71*.

Jin, D-H (2006). *Investigation on refrigerant distribution in evaporator manifolds*. [Doctoral Thesis, University of Maryland, College Park]. University of Maryland, College Park ProQuest Dissertations Publishing, 2006. 3222501, 16. https://www.proquest.com/openview/6678e938c207a5603c9bf1c46cfac0af/1?pq-origsite=gscholar&cbl=18750&diss=y

Kim, C.-H., Kim, N.-H. (2021). An experimental study of refrigerant distribution in an automotive condenser. *Applied Thermal Engineering, 184,* 116259..

Kim, M. S., Lee, K. S., Song, S. (2008). Effects of pass arrangement and optimization of design parameters on the thermal performance of a multi-pass heat exchanger. *International Journal of Heat and Fluid Flow*, *29*(1).

Lalot, S., Florent, P., Lang, S. K., Bergles, A. E. (1999). Flow maldistribution in heat exchangers. *Applied Thermal Engineering*, *19*(8).

Lee, K-S., Oh, S-J. (2004). Optimal shape of the multi-passage branching system in a single-phase parallel-flow heat exchanger. *International Journal of Refrigeration*, *27*(1).

Li, W., Tu, J., Liu, Y., Wang, D., Shi, J., Chen, J. (2021). Design and experimental validation of a new condenser of an automotive air conditioning unit to address non-uniform air velocity distributions. *International Journal of Refrigeration*, *131*.

Liu, M., Jiang, C., Khoo, B. C., Zhu, H., Gao, G. (2024). A cell-based smoothed finite element model for the analysis of turbulent flow using realizable k-ε model and mixed meshes. *Journal of Computational Physics*, *501*.

Nagata, K., Katsuta, M., Kim, J. S., Sakuma, T. (Nov 1988). *Two Phase Flow Distribution in Serpentine Type Evaporator (First Report : Non-Heating Mode)*. KSME/JSME THERMAL and FLUID Engineering Conference, Seoul, South Korea. https://www.dbpia.co.kr/Journal/articleDetail?nodeId=NODE00326727

Rao, B. P., Das, S K. (2004). An Experimental Study on the Influence of Flow Maldistribution on the Pressure Drop Across a Plate Heat Exchanger. *Journal of Fluids Engineering*, *126*(4).

Rao, Bobbili, P., Sunden, B., Das, S. K. (2006). Thermal analysis of plate condensers in presence of flow maldistribution. *International Journal of Heat and Mass Transfer*, *49*(25–26).

Shirzadi, M., Mirzaei, P. A., Naghashzadegan, M. (2017). Improvement of k-epsilon turbulence model for CFD simulation of atmospheric boundary layer around a high-rise building using stochastic optimization and Monte Carlo Sampling technique. *Journal of Wind Engineering and Industrial Aerodynamics*.

Shojaeefard, M., Molaeimanesh, G., Yarmohammadi, A., Changizian, S. (2017). Multi-objective optimization of an automotive louvered fin-flat tube condenser for enhancing HVAC system cooling performance. *Applied Thermal Engineering*.

Shojaeefard, M. S., Nourbakhsh, S. D., Zare, J. (2017). An investigation of the effects of geometry design on refrigerant flow mal-distribution in parallel flow condenser using a hybrid method of finite element approach and CFD simulation. *Applied Thermal Engineering*, *112*.

The Chemours Company FC, LLC. (2018). *Thermodynamic Properties of Opteon™ YF*. https://www.opteon.com/en/-/media/files/opteon/opteon-yf-thermodynamic-properties-si.pdf?rev=8fa3ce05a4fa4573b9b6750afebecd0e

Thonon, B., Mercier, P., Feidt, M. (1992). *Flow Distribution in Plate Heat Exchangers and Consequences on Thermal and Hydraulic Performances.* In: Roetzel, W., Heggs, P.J., Butterworth, D. (eds) Design and Operation of Heat Exchangers. EUROTHERM Seminars, vol 18. Springer, Berlin, Heidelberg.

Tompkins, D. M., Yoo, T., Hrnjak, P., Newell, T., Cho, K. (2002). Flow Distribution and Pressure Drop In Microchannel Manifolds. *International Refrigeration and Air Conditioning Conference*, *Paper 554*, Purdue University.

Tuo, H., Hrnjak, P. (2013). Effect of the header pressure drop induced flow maldistribution on the microchannel evaporator performance. *International Journal of Refrigeration*, *36*(8).

Vist, S., Pettersen, J. (2004). Two-phase flow distribution in compact heat exchanger manifolds. *Experimental Thermal and Fluid Science*, *28*(2–3).

Wang, T., Gu, B., Wu, B., Ma, H., Qian, C. (2015). Modeling for multi-pass parallel flow condenser with the effect of refrigerant mal-distribution. *International Journal of Refrigeration*, *60*.

Yan, Y. Y., Lin, T. F. (1999). Condensation heat transfer and pressure drop of refrigerant R-134a in a small pipe. *International Journal of Heat and Mass Transfer*, *42*(4).

Zhao, Y., Liang, Y., Sun, Y., Chen, J. (2012). Development of a mini-channel evaporator model using R1234yf as working fluid. *International Journal of Refrigeration*, *35*(8).

Zou, Y., Hrnjak, P S. (2013). Experiment and visualization on R134a upward flow in the vertical header of microchannel heat exchanger and its effect on distribution. *International Journal of Heat and Mass Transfer*, *62*.

Zou, Y., Hrnjak, P. S. (2013). Refrigerant distribution in the vertical header of the microchannel heat exchanger – Measurement and visualization of R410A flow. *International Journal of Refrigeration*, *36*(8).

Zou, Y., Tuo, H., Hrnjak, P S. (2014). Modeling refrigerant maldistribution in microchannel heat exchangers with vertical headers based on experimentally developed distribution results. *Applied Thermal Engineering*, *64*(1–2).